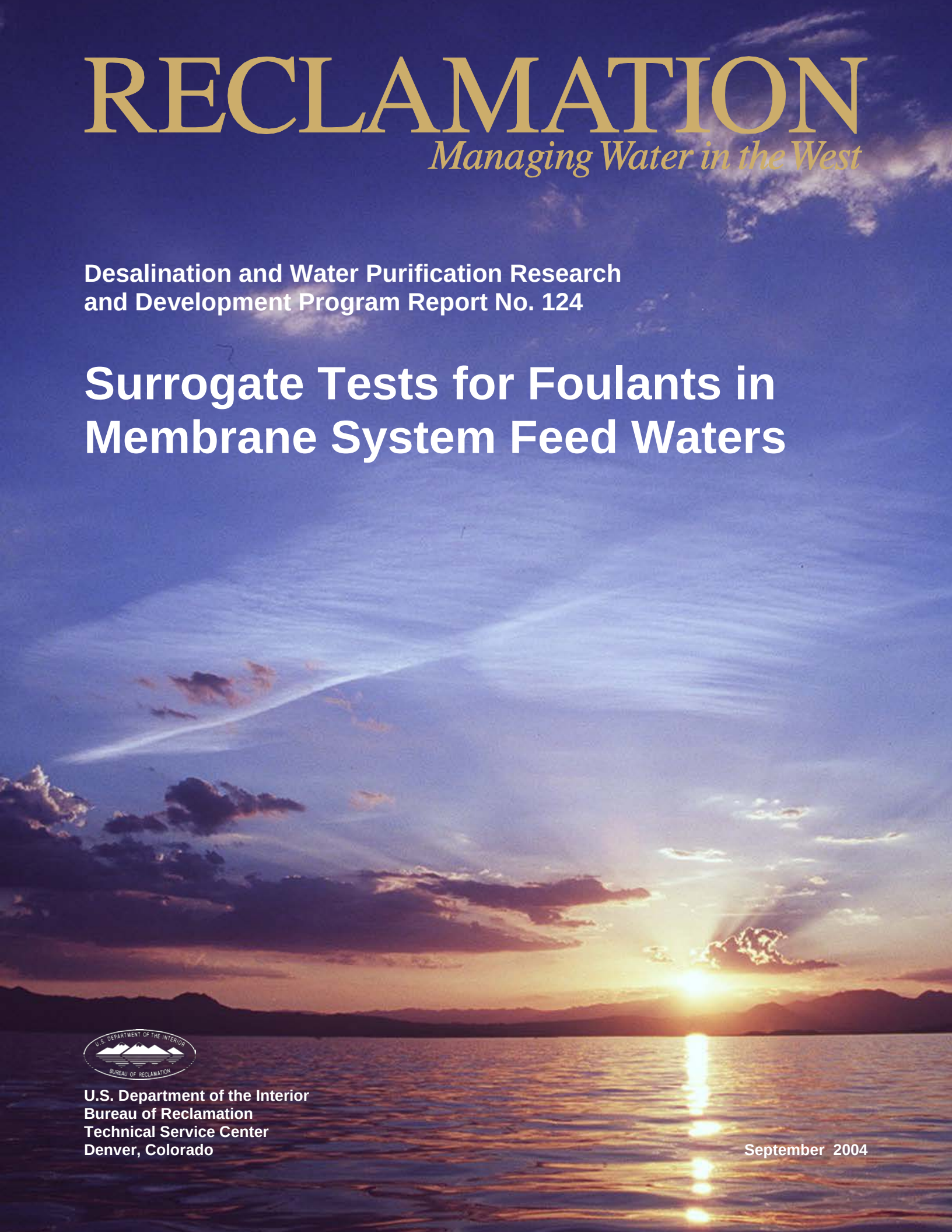

RECLAMATION

Managing Water in the West

Desalination and Water Purification Research and Development Program Report No. 124

Surrogate Tests for Foulants in Membrane System Feed Waters

U.S. Department of the Interior
Bureau of Reclamation
Technical Service Center
Denver, Colorado

September 2004

REPORT DOCUMENTATION PAGE	Form Approved OMB No. 0704-0188

PLEASE DO NOT RETURN YOUR FORM TO THE ABOVE ADDRESS.

1. REPORT DATE *(DD-MM-YYYY)*	2. REPORT TYPE	3. DATES COVERED *(From - To)*
September 2004	Final	January 2001 - September 2004

4. TITLE AND SUBTITLE	5a. CONTRACT NUMBER
Surrogate Tests for Foulants in Membrane Systems Feed Waters	5b. GRANT NUMBER
	5c. PROGRAM ELEMENT NUMBER
6. AUTHOR(S)	5d. PROJECT NUMBER
Gary Amy, John Pellegrino, NoWha Lee, Chalor Jarusutthirak and Namguk Her	5e. TASK NUMBER
	5f. WORK UNIT NUMBER

7. PERFORMING ORGANIZATION NAME(S) AND ADDRESS(ES)	8. PERFORMING ORGANIZATION REPORT NUMBER
Department of Civil, Environmental and Architectural Engineering, University of Colorado Boulder, CO 80309-0424	
9. SPONSORING/MONITORING AGENCY NAME(S) AND ADDRESS(ES)	**10. SPONSOR/MONITOR'S ACRONYM(S)**
Bureau of Reclamation, Denver Federal Center, P.O. Box 25007, Denver, CO 80225	USBR
	11. SPONSOR/MONITOR'S REPORT NUMBER(S) DWPR No. 124

12. DISTRIBUTION/AVAILABILITY STATEMENT

Available from https://www.usbr.gov/research/dwpr/DWPR_Reports.html

This project was initiated with the objective of developing and applying new innovative analytical tools to identify and characterize organic fouling in both low pressure (MF/UF) and high pressure (NF/RO) membranes. These analytical tools represent surrogate parameters that are intended to capture the signature of bulk organic matter in various forms.

15. SUBJECT TERMS

Desalination,fouling, microfiltration, nanofiltration, ultrafiltration, reverse osmosis.

16. SECURITY CLASSIFICATION OF:			17. LIMITATION OF ABSTRACT	18. NUMBER OF PAGES	19a. NAME OF RESPONSIBLE PERSON
a. REPORT	b. ABSTRACT	a. THIS PAGE			Yuliana Porras-Mendoza
U	U	U	SAR		19b. TELEPHONE NUMBER *(Include area code)* 303-445-2265

Standard Form 298 (Rev. 8/98)
Prescribed by ANSI Std. Z39.18

Mission Statements

The mission of the Department of the Interior is to protect and provide access to our Nation's natural and cultural heritage and honor our trust responsibilities to Indian Tribes and our commitments to island communities.

The mission of the Bureau of Reclamation is to manage, develop, and protect water and related resources in an environmentally and economically sound manner in the interest of the American public.

Disclaimer

Information contained in this report regarding commercial products or firms was supplied by those firms. It may not be used for advertising or promotional purposes and is not to be construed as an endorsement of any product or firm by the Bureau f Reclamation.

The information contained in this report was developed for the Bureau of Reclamation; no warranty as to the accuracy, usefulness, or completeness is expressed or implied.

Desalination and Water Purification Research and Development Report No. 124

Surrogate Tests for Foulants in Membrane System Feed Waters

Gary Amy
John Pellegrino
NoWha Lee
Chalor Jarusutthirak
Namguk Her
Department of Civil, Environmental and Architectural Engineering
University of Colorado
Boulder, CO 80309-0424

MAST Project No. 01-2

Contents

List of Figures

List of Tables

Acronyms

AOM	atomic force microscopy
AFM	attenuated total reflection-Fourier transform infrared spectroscopy
ATR-FTIR EEM	fluorescence excitation-emission matrix
EfOM	effluent organic matter
HPI	hydrophilic
HPO	hydrophobic
IMS	integrated membrane system
MW	molecular weight
NOM	natural organic matter
OM	bulk organic matter
PEG	polyethylene glycol
PWP	pure water permeability
SEM SUVA	scanning electron microscopy
TPI	specific ultraviolet absorbance
	transphilic

1. Executive Summary

This project was initiated with the objective of developing and applying new innovative analytical tools to identify and characterize organic fouling in both low pressure (MF/UF) and high pressure (NF/RO) membranes. These analytical tools represent surrogate parameters that are intended to capture the signature of bulk organic matter (OM) in various forms including natural (NOM), algal (AOM), and wastewater effluent (EfOM) organic matter, elucidating the size, structure, and functionality of OM. The tools include: (i) specific UV absorbance (SUVA), indicating the aromatic versus aliphatic character of OM; (ii) size exclusion chromatography with on-line dissolved organic carbon detection (SEC-DOC), reflecting the molecular weight (MW) or size distribution of OM; (ii) fluorescence excitation-emission matrix (EEM), distinguishing between humic-like and protein-like OM; (iv) and XAD-8/-4 resin adsorption chromatography, describing the polarity distribution according to hydrophobic (HPO), transphilic (TPI), and hydrophilic (HPI) OM. In order to further understand the nature of organic foulants deposited on/in the membrane surface/pores, other analytical tools were used to probe fouled membrane specimens including: (i) attenuated total reflection-Fourier transform Infrared Spectroscopy (ATR-FTIR), revealing the functionality of OM deposited on a membrane surface; (ii) atomic force microscopy (AFM), describing the topography and pore distribution of a membrane surface; and (iii) scanning electron microscopy (SEM), permitting visualization of foulants on a membrane surface. In order to under stand OM-membrane interactions, important membrane properties were also determined including pure water permeability (PWP), pore size/molecular weight cutoff (MWCO), zeta potential (an index of surface charge), and contact angle (an index of hydrophobicity). The report is written in two parts: the first addresses low pressure (MF/UF) membranes while the second highlights high pressure (NF/RO) membranes. The results support the premise that the surrogate parameters reveal fouling potential, with fouling correlated with a high MW SEC peak, protein-like OM, HPI OM, and/or low SUVA.

2. Introduction

A major premise of this work is that new, innovative analytical techniques (or innovative interpretation approaches using classical techniques) can better define organic matter (OM) fouling of membranes, quantify membrane fouling potential, as well as provide insight into actual fouling mechanisms associated with many types of organic foulants. The analytical techniques elucidate the size, structure, and functionality of OM, and thus provide insight into OM-membrane interactions, with characterization of important membrane properties providing further insight. An important focus of this work has been the evaluation of distinct OM "types" derived from different sources, including allochthonous natural organic matter (NOM), derived from terrestrial sources (e.g., vegetative debris); autochthonous NOM or algal organic matter (AOM) derived from extracellular and intracellular materials produced upon algal cell lysis; and wastewater effluent organic matter (EfOM) derived from soluble microbial products produced during secondary biological treatment. Our OM analytical techniques provide unique signatures for NOM, AOM, and EfOM. Contrary to the literature, we believe that allochthonous (humic-like) NOM is less problematical as a foulant compared to AOM and EfOM of a microbial origin, with the latter exhibiting protein- and polysaccharide-like signatures. It is also reasonable to expect different fouling mechanisms for low pressure versus high pressure membranes, given differences in pore size and membrane materials. In Part I of this report, we focus on low pressure (MF/UF) membranes and organic matter (OM) in two forms: bulk OM and OM isolates. In Part II, we highlight high pressure membranes and bulk OM.

3. Part I: Identification of Organic Foulants and Fouling Mechanisms in Low Pressure (MF/UF) Membranes

3.1 Introduction

Low pressure membranes are employed for particle and microorganism rejection in drinking water and wastewater applications. When coupled with a high pressure membrane in an integrated membrane system (IMS), the low pressure membrane serves as a pretreatment step for the high pressure membrane. In removing particles, a reversible cake layer builds up and is easily displaced during periodic backwashing. A problem arises from smaller colloids that can block pores or macromolecules that mat constrict pores.

The low pressure membrane effort first addressed natural waters containing bulk OM and then focused on OM isolates/fraction studied within the context of synthetic waters. In the former work, the analytical techniques helped identify problematical fractions of OM as foulants, while the latter work confirmed that certain OM isolates/fractions are problematical.

3.2 Bulk Organic Matter

3.2.1 Materials and Methods

Membranes and Filtration Apparatus. Four different membranes were used in (constant pressure) flux decline tests for the study of NOM fouling (Table 1); two MF and two UF membranes possessing hydrophilic (HPI) or hydrophobic (HPO) properties (surmised from contact angle measurements—generally, a contact angle of over 50° is considered as hydrophobic.) Each membrane was anticipated to show different trends of membrane flux-decline depending on NOM characteristics and membrane properties. NOM flux decline tests were performed using a dead-end stirred-cell filtration unit that was connected to a feed reservoir and a nitrogen gas tank. After feed water is introduced into the cell, permeate discharges from the bottom of the cell and retentate accumulates in the cell under applied pressure, thus simulating dead-end filtration.

Water Quality of Source (Feed) Waters. Four natural waters were selected for studying NOM fouling with the four different low-pressure membranes. The results include studies of membrane fouling with four French surface waters; Marne River, Cazau Lake, La Bultière Reservoir and Yffiniac River. The Marne River is in the Paris area, Cazau Lake is close to Bordeaux, La Bultière Reservoir is near Vendée, and Yffiniac River is in Brittany. The water quality of these source (feed) waters is summarized in Table 2. Each sample was pre-filtered with a 0.45μm filter. The Cazau

Lake water exhibits a low SUVA value compared to other source waters. The Marne River water contained a relatively high concentration of Ca^{2+}.

Table 1 Specifications and Properties of Membranes

Membrane Type	UF		MF	
	Hydrophobic	Hydrophilic	Hydrophobic	Hydrophilic
Membrane code	PES, Orelis	YM100, Millipore	GVHP, Millipore	GSWP, Millipore
Pore size	100KD	100KD	0.22μm	0.22μm
Materials	PES	Regenerated Cellulose	PVDF	Mixed Cellulose Ester
Pure water permeability	5.15 (gal/ft2-day-psi) 122 (L/m2-hrs-bar)	15.7 (gal/ft2-day-psi) 372 (L/m2-hrs-bar)	36.1 (gal/ft2-day-psi) 856 (L/m2-hrs-bar)	158.9 (gal/ft2-day-psi) 3770 (L/m2-hrs-bar)
Contact angle	58°	18°	83°	19°
Zeta potential *	-32mV	-3mV	-7mV	20mV

* at pH 7.0 and 10mM KCl

Table 2. Water Quality of French Source (Feed) Waters

Source	Marne River	Cazau Lake	Bultière Reservoir	Yffiniac River
DOC (mg/L)	2.7	4.99	6.86	8.42
UVA_{254} (cm^{-1})	0.057	0.069	0.177	0.295
SUVA (L/mg·m)	2.1	1.4	2.6	3.5
pH	8.49	7.12	7.27	7.53
Conductivity (μS/cm)	384	183	233	308
Ca^{2+} (mg/L)	38.8	4.8	21.4	14.8
Fe (mg/L)	≤ MDL	0.005	≤ MDL*	≤ MDL
Si (mg/L)	1.06	0.03	0.68	5.78
Mn (mg/L)	≤ MDL	≤ MDL	0.04	≤ MDL

* MDL: method detection limit (0.002ppm for Fe; 0.001ppm for Mn)

NOM Characterization. Molecular weight (MW) distributions were determined by a HPSEC (High Pressure Size Exclusion Chromatography) method. A high performance liquid chromatograph (HPLC, LC600 Shimadzu) was used with UVA (SPD-6A Shimadzu) and on-line DOC detectors (modified Sievers Turbo Total Organic Carbon

Analyzer) following size separation by a HW-50S column. The column packing material is a Toyopearl resin, semi-rigid, spherical beads with a hydrophilic surface that are synthesized by co-polymerization of ethylene glycol and methacrylate-type polymers (GROM, Denmark). The separation capacity of the column is 100 ~ 18,000 dalton based on polyethylene glycols (PEGs), and 500 ~ 80,000 dalton with globular proteins. HW-65S column was also used for investigating of larger size of molecules. The separation capacity of the column is 500 ~ 10^6 dalton based on PEGs and 40000 ~ 5×10^6 dalton. The DOC detector is connected to the UVA detector waste line sequentially. UVA and DOC data are recorded every 6 seconds by a modified Labview software. The SEC column separates compounds based on hydrodynamic molecular size. The average retention time is affected by the effective size and structure of the molecules. Consequently, larger and linear shaped molecules are excluded earlier than smaller and globular shape molecules (Her et al., 2002). Polyethylene glycols (PEGs) were used for calibration of the relationship between MW and retention time.

XAD polymeric resins have been developed for the isolation of humic substances and other organic compounds from water. Typically, NOM can be separated into three fractions by the XAD-8/-4 resin fractionation technique: the hydrophobic (HPO) fraction which is XAD-8 adsorbable, the transphilic (TPI) fraction which is XAD-4 adsorbable, and hydrophilic (HPI) fraction which passes through the XAD-8/-4 resin without any adsorption. The colloid fraction ends up in the hydrophilic fraction when dialysis is not used in advance to pre-isolate colloids (discussed in a succeeding section).

The source waters were filtered with 0.45μm filters and adjusted to pH 2 before being passed through XAD-8 and XAD-4 in sequence. Table 3 shows XAD 8/4 resin fractionation results. Each fraction was determined by performing a DOC mass balance across XAD-8/-4 resin columns after acidification to pH 2.0. The Marne and Yffiniac River waters showed a very typical composition of fractions (hydrophobic (HPO): ~50%, transphilic (TPI): ~25%, hydrophilic (HPI): ~25%) while Cazau Lake and Bultière Reservoir waters each contained a relatively low hydrophobic fraction and a relatively high hydrophilic fraction.

Table 3. XAD-8/-4 Fractionation of Source (feed) Water

Source Water	Hydrophobic DOC (%)	Transphilic DOC (%)	Hydrophilic DOC (%)
Marne River	50	22	28
Cazau Lake	39	25	35
Bultière Reservoir	44	26	31
Yffiniac River	48	28	24

Morphological Analyses. Microscopy represents a powerful technique to visualize directly the structural appearance of MF and UF membrane surfaces. Scanning electron microscopy (SEM) and atomic force microscopy (AFM) have been employed for morphological analyses. SEM has been widely used for surface analysis. It produces topographical images of the membrane surface. SEM images provide direct, practical and

structural membrane information. The spatial image is recorded by capture of secondary electrons reflected from the sample specimen. The membrane specimens are sputter-coated with Au and grounded to prevent negative charging.

AFM is a scanning probe microscope (Zeman and Zydney, 1996). A very fine tip probes the material surface directly and generates three-dimensional maps of undulation. The pore image reflects convolution of pore shape and the tip shape when the size of an AFM probe tip is comparable to the size of the pore. AFM measures the pore maximum diameter at the membrane surface when the pore sizes are irregular in an actual membrane. The AFM utilized is made by Digital instruments, and data are analyzed with a computer program (nanoscope II). The tip size is 4~10nm and is made of an etched single crystal silicon. Clean membrane specimens were prepared with MQ water filtration and dried at room temperature to remove covered materials, and fouled membrane specimens were dried at room temperature. While the drying procedure may cause a slight distortion of the membrane surface, the morphology was compared against a dried clean membrane after MQ washing, side by side, providing a qualitative and semi-quantitative comparison.

3.2.2 Results and Discussion

Flux Decline Tests. Flux decline tests were performed to investigate fouling in low-pressure membranes by natural organic matter, which has been revealed as a major foulant. Applied pressure varied depending on the membrane: PES (UF-HPO) at 14 psi (1 bar); YM100 (UF-HPI) at 6 psi (0.43 bar); GVHP (MF-HPO) at 4 psi (0.29 bar); and GSWP (MF-HPI) at 4 psi (0.29 bar). The initial flux upon applied pressure was dependant on water source, as displayed in Table 4.

Figure 1 illustrates flux decline with the four source waters based on time; Table 5 quantifies flux decline based on delivered DOC (cumulative feed-water DOC mass per unit area of membrane surface = feed water DOC (mg/L) × cumulative volume (L) / membrane surface (m^2)) after 60 minutes of membrane filtration. The Cazau Lake and Bultière Reservoir waters, containing a greater hydrophilic fraction, showed greater flux decline than that of the Marne River and Yffiniac River waters containing a greater hydrophobic fraction. Even though the DOC concentration of Cazau Lake water is less than Bultière Reservoir and Yffiniac River waters, Cazau Lake water showed the most significant flux decline (up to 73%), except for the PES (UF-HPO) membrane. Thus, waters with a high content of hydrophilic (HPI) fraction resulted in more significant flux decline. It is noteworthy that organic colloids generally pass through the XAD-4/-8 resins and end up in the hydrophilic fraction when colloids are not pre-isolated with dialysis before XAD-4/-8 resin fractionation (Laabs, 2003). The hydrophilic (HPI) fraction content of a feed water may be a predictor of fouling of low pressure membranes.

Table 4. Initial Flux of Each Source Water with Various Membranes.

Membrane	Pressure	J_0-Feed water ($L/m^2 \cdot h$)			
		Marne River	Cazau Lake	Bultiere Reservoir	Yffiniac River
PES (UF-HPO)	14 psi	111	294	159	159
YM100 (UF-HPI)	6psi	191	207	119	151
GVHP (MF-HPO)	4psi	183	207	103	278
GSWP (MF-HPI)	4psi	954	835	1033	1113

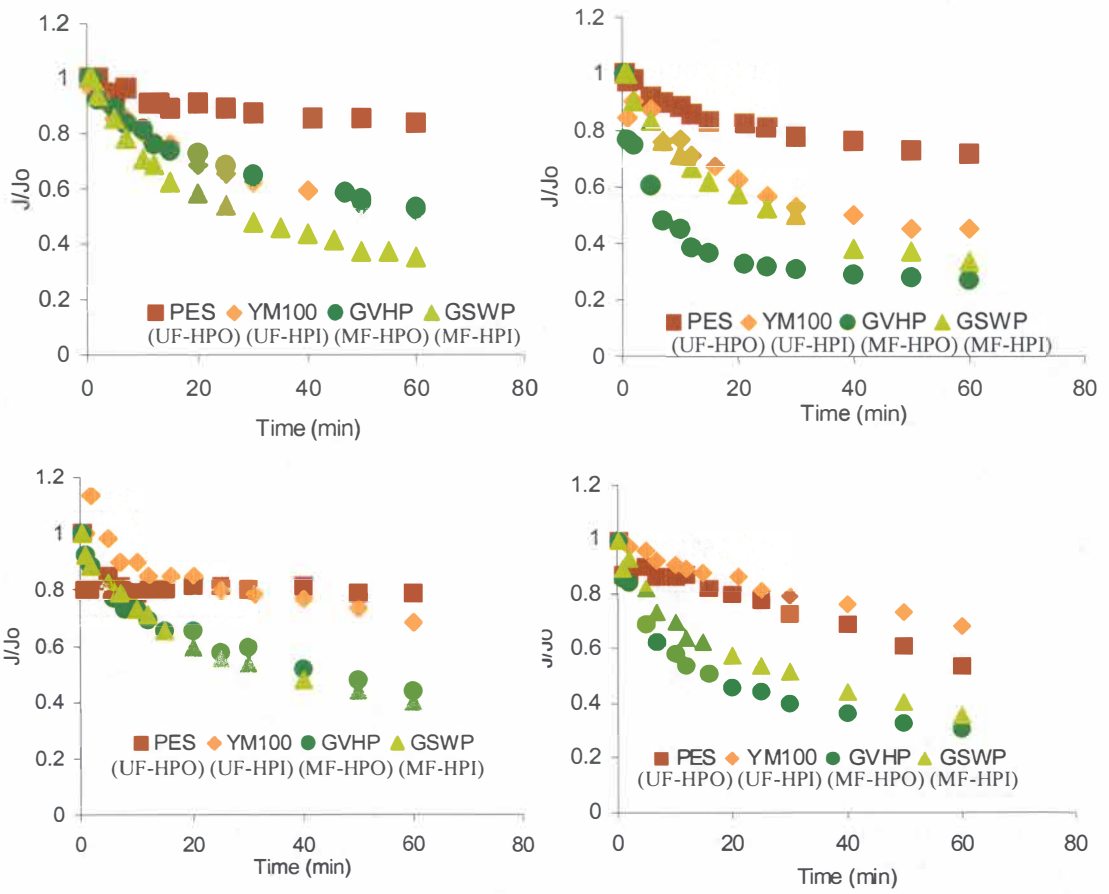

Figure 1. Flux decline curves with source waters (Top: Marne river (left), Cazau lake (right); Bottom: Bultière Reservoir (left), Yffiniac River (right))

Figure 2 illustrates flux decline trends of each membrane based on delivered DOC. UF membranes generally showed less flux decline than MF membranes. The GVHP (MF-HPO) showed the most significant flux decline as a function of delivered DOC while the GSWP (MF-HPI) accommodated the highest delivered DOC. However, distinctive

differences in flux decline between hydrophobic and hydrophilic membranes were not observed suggesting that other membrane properties may be more influential.

Identification of Foulants with Chemical Analyses. Source (feed) waters and corresponding membrane permeates were analyzed by SEC-DOC/UV. Figures 3, 4, 5 and 6 show the SEC–DOC and –UV responses of source waters based on the relative MW distribution determined by PEG standards. The first peak is typically assumed to be proteins and/or polysaccharides, the second peak is humic substances, and the third is low molecular weight organic acids (Huber et al., 1998, Her et al., 2000). The Cazau Lake and Bultière Reservoir waters show a relatively high intensity of the first peak compared to the other waters. Both of these waters are a lake or a reservoir and contain a greater hydrophilic (HPI) fraction. The first peaks are reduced effectively in most of the membrane filtrations due to their large molecular weight. These large molecular weight peaks correspond to macromolecular compounds and/or colloidal organic matter, and contribute to significant organic fouling during low pressure membrane filtration.

Table 5. Flux Decline of Source (Feed) Waters

Membrane		Marne River	Cazau Lake	Bultière Reservoir	Yffiniac River
YM100 (UF-HPI)	Time (60min)	48% (≈333mg/m^2)	55% (≈570mg/m^2)	32% (≈652mg/m^2)	32% (≈1020mg/m^2)
	Delivered DOC (≈250mg/m^2)	41% (40min)	37% (20min)	15% (20min)	11% (12min)
PES (UF-HPO)	Time (60min)	16% (≈265mg/m^2)	28% (≈1121mg/m^2)	21% (≈877mg/m^2)	46% (≈958mg/m^2)
	Delivered DOC (≈250mg/m^2)	16% (60min)	14% (12min)	20% (15min)	12% (12min)
GSWP (MF-HPI)	Time (60min)	65% (≈1354mg/m^2)	67% (≈2013mg/m^2)	60% (≈3924mg/m^2)	64% (≈4892mg/m^2)
	Delivered DOC (≈250mg/m^2)	22% (7min)	17% (5min)	12% (2min)	7% (2min)
GVHP (MF-HPO)	Time (60min)	47% (≈327mg/m^2)	73% (≈344mg/m^2)	56% (≈410mg/m^2)	69% (≈1015mg/m^2)
	Delivered DOC (≈250mg/m^2)	41% (47min)	71% (40min)	40% (30min)	42% (10min)

( ): Delivered DOC

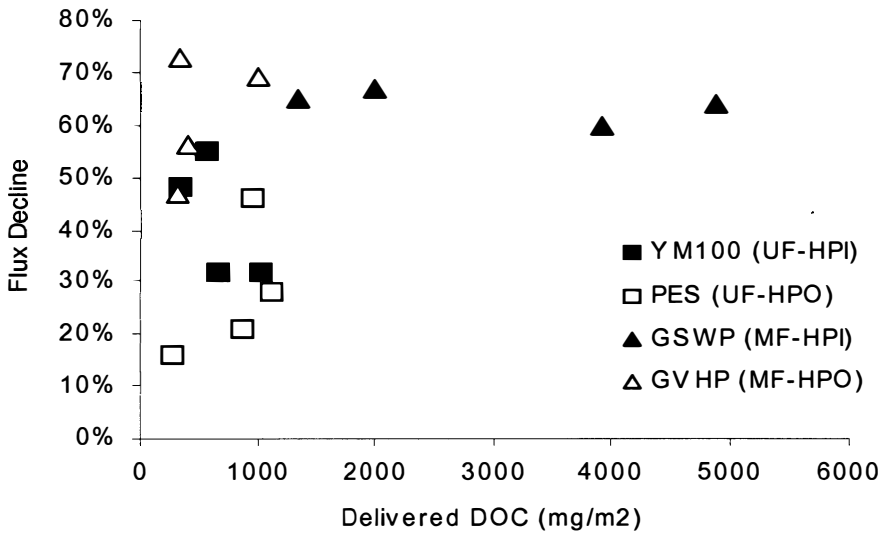

Figure 2. Flux Decline of Source (Feed) Waters with Different Membranes based on Delivered DOC

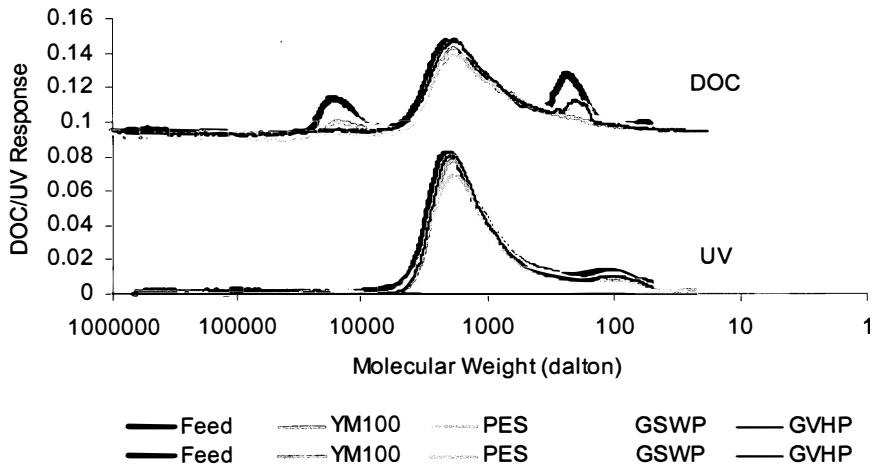

Figure 3. SEC-DOC distribution of Marne River Water NOM based on MW

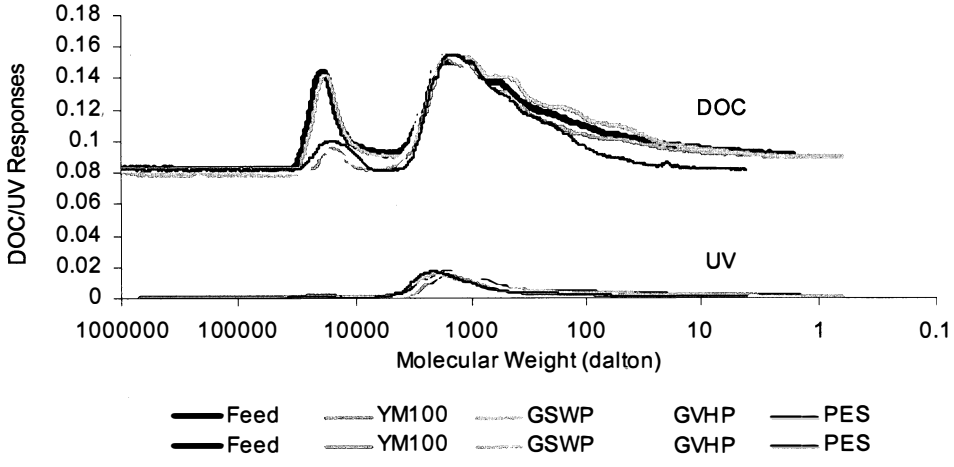

Figure 4. SEC-DOC distribution of Cazau Lake water based on MW

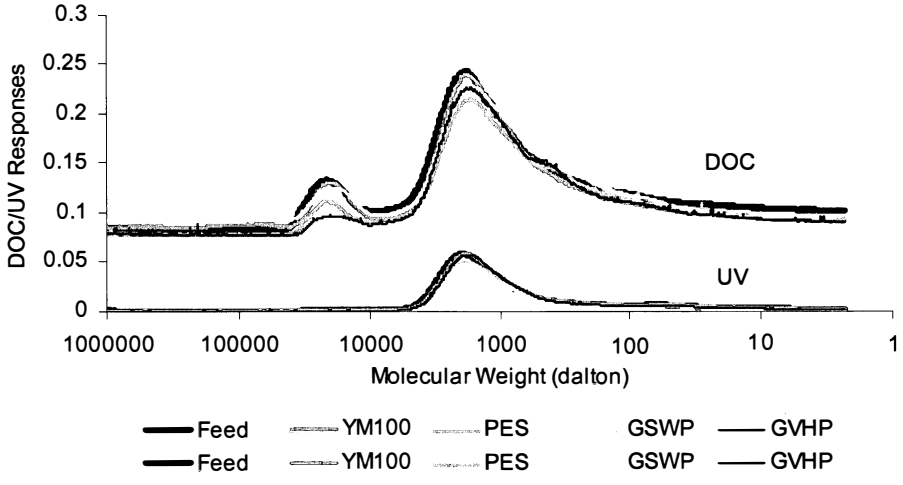

Figure 5. SEC-DOC Distribution of Bultière Reservoir Water NOM based on MW

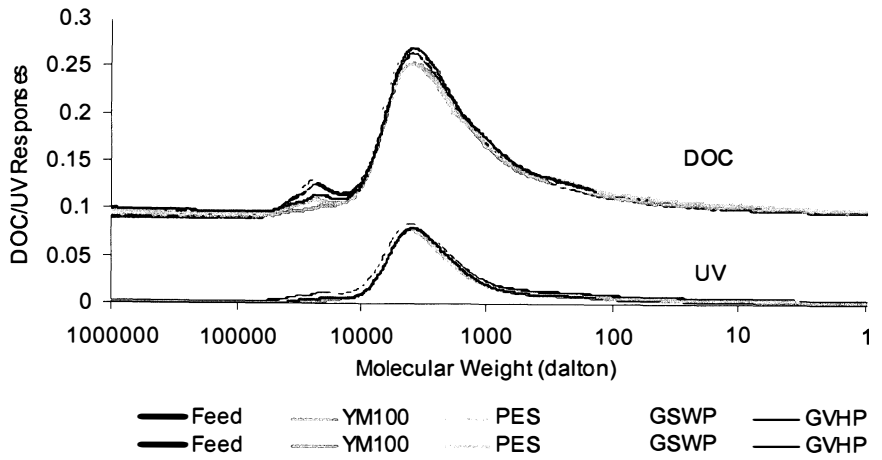

Figure 6. SEC-DOC Distribution of Yffiniac River Water NOM based on MW

ATR-FTIR Analysis. FTIR analysis was performed to determine whether rejected organic compounds were found on, and retained by, the membrane surface. This approach was not very informative for low pressure membranes due to their large pore size and different fouling mechanism(s) compared to high pressure (NF or RO) membranes where FTIR has been successfully employed (Her et al., 2000 and Jarusutthirak, 2002). However, as shown in Figure 7, the FTIR analysis of the PES (UF-HPO) membrane filtered with Cazau lake water indicated a specific peak at around 1070 cm^{-1}. This corresponds to C-O stretching vibration in alcohol and phenol (1260-1000 cm^{-1}). The OH stretching vibrations of the SiOH group are observed in a similar region (830-1110 cm^{-1} and 3700-3200 cm^{-1}) but the Cazau lake water contains the lowest Si concentration among source (feed) waters and a high content of macromolecules with SEC-DOC/UV analysis. Thus, the peak is more attributable to C-O stretching vibration associated with polysaccharides. As Jarusutthirak et al. (2002) and Reichenbach et al. (2001) observed with high (RO and NF) and low (MF and UF) pressure membranes, polysaccharides and/or proteins in macromolecular and/or colloidal forms contribute to significant membrane fouling, rather than inorganic fouling as indicated by Howe et al (2002).

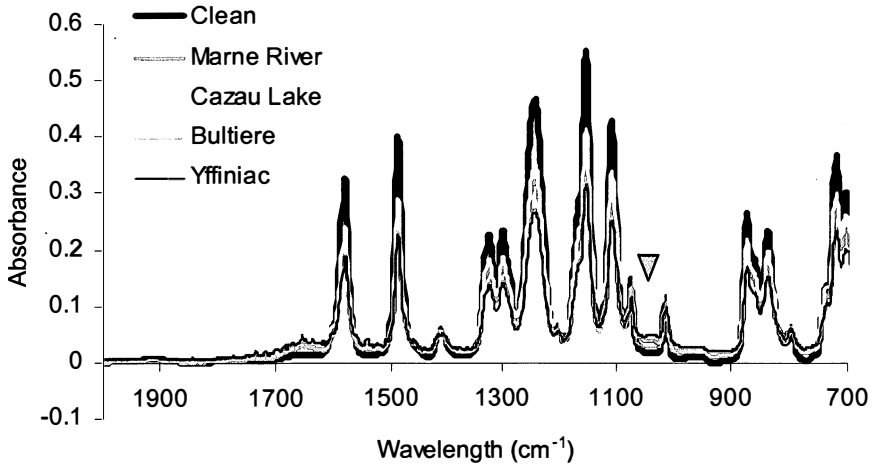

Figure 7. FTIR Analysis of PES Membrane with Source (Feed) Waters.

Morphological Analysis. Atomic force microscopy (AFM) and scanning electronic microscopy (SEM) analyses were performed to compare morphological changes between clean and fouled membranes. Figure 8 compares the AFM surface image (top view) and side view of clean membranes. The UF membranes show a smoother surface than the MF membranes, and generally imparted less flux decline. The PES (UF-HPO) membrane exhibited the least roughness compared to other membranes and showed the least flux decline in each case.

Figure 9 displays 3-D views of the YM100 (UF-HPI) and Figure 10 shows section analyses of the GVHP (MF-HPO) comparing clean and fouled membranes, respectively. From the left image, the clean membrane, the membrane fouled with Yffiniac river water, and the membrane fouled with Bultière Reservoir water are sequentially shown. The fouled membrane surfaces appear smoother than the corresponding clean membrane surfaces, and exhibit a surface coverage with a "higher topography" The AFM images of UF membranes clearly support the notion of surface coverage as a fouling mechanism. In contrast, the AFM images of MF membranes indicate a different fouling mechanism for MF membranes (i.e., pore blockage) by section analyses. From the section analysis (Figure 10), the AFM "valleys" have largely disappeared for the fouled membranes; this is likely due to filling of the membrane pore structure with foulant material. AFM analyses elucidate that the membrane roughness of each membrane is very different and may be more influential in membrane fouling by controlling interaction between molecules and the membrane surface or structure than the hydrophobic/hydrophilic character of membranes.

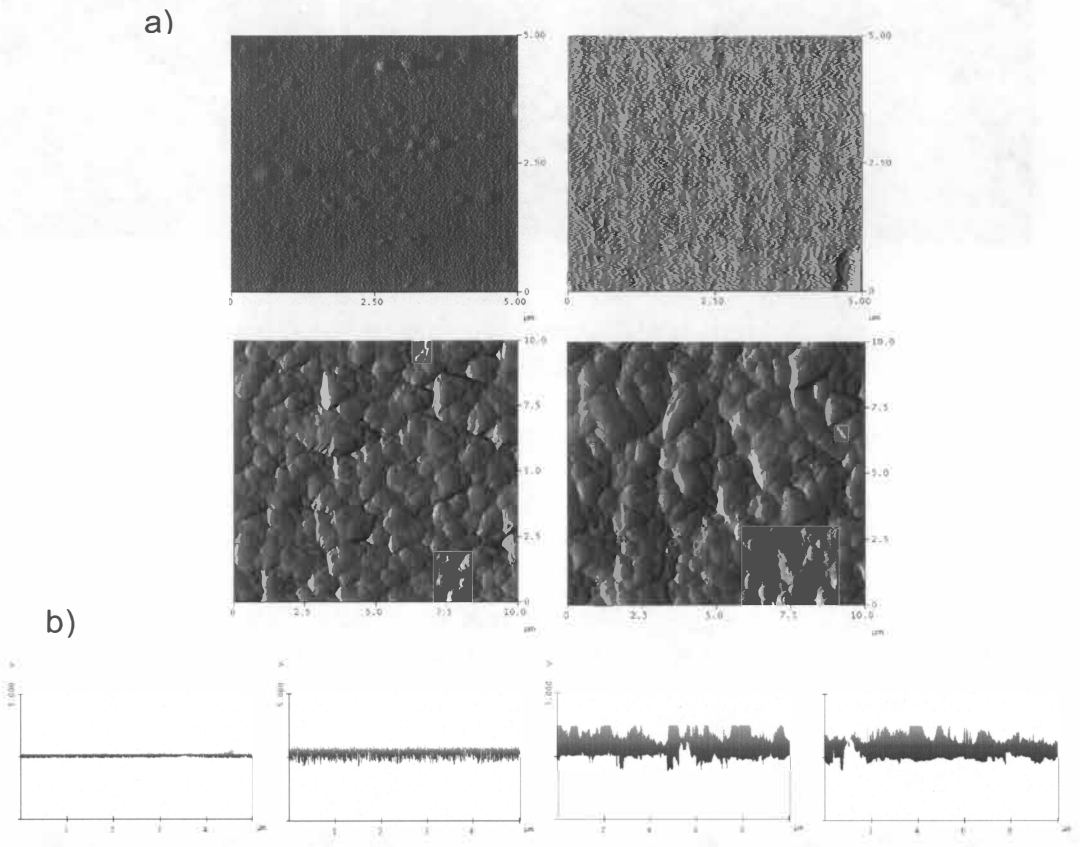

Figure 8. Surface View (a) and Side View (b) of Clean Membranes by AFM (from the left: YM100 (UF-HPI), PES (UF-HPO), GSWP (MF-HPI), GVHP (MF-HPO); scan size: UF 5μm; MF 10μm, 5.000V = 250nm)

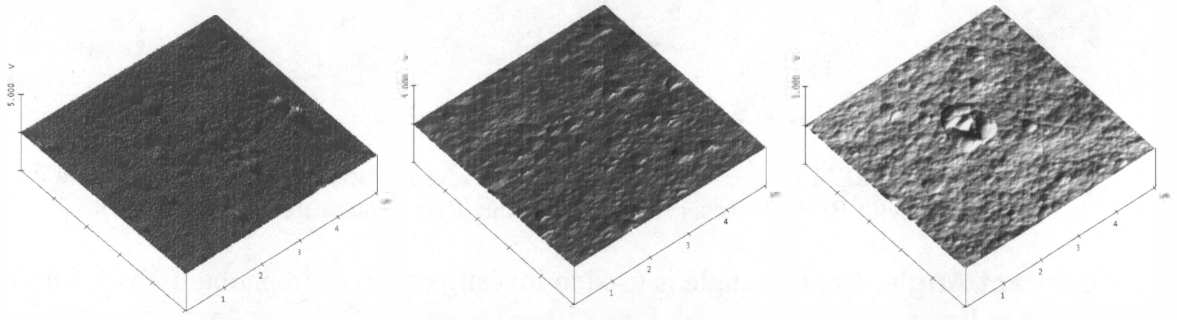

Figure 9. 3D Views of UF membrane Surfaces by AFM (membrane: YM100 (UF-HPI); from the left: clean, Yffiniac River and Bultière Reservoir)

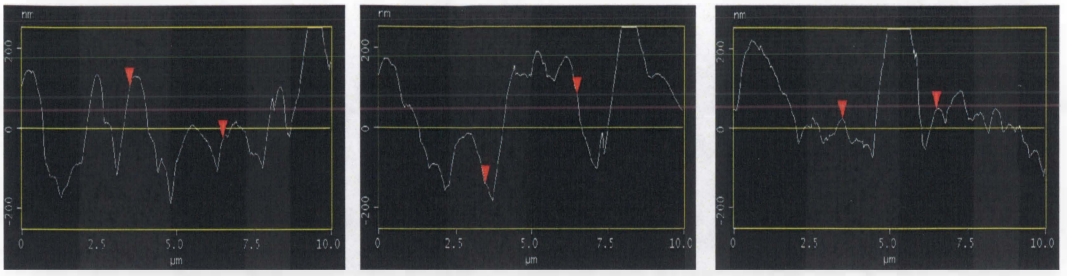

Figure 10. Section Analysis of MF Membrane Surface by AFM (membrane: GVHP (MF-HPO); from left: Clean, Yffiniac River and Bultière Resevoir)

SEM images provide additional detailed structural features of MF membranes. Figure 11 reveals that the pores of the GSWP (MF-HPI) membrane filtered with Bultière Reservoir and Yffiniac river water were reduced after filtration, suggesting that the pores were blocked by NOM materials. This phenomenon may be attributable to adsorption of NOM around membrane pores by smaller molecules (i.e., pore constriction) and/or pore blockage by larger molecules and/or colloids. Thus, membrane fouling mechanisms are not only a function of membrane type (MF vs. UF), but also depend on source (feed) water characteristics.

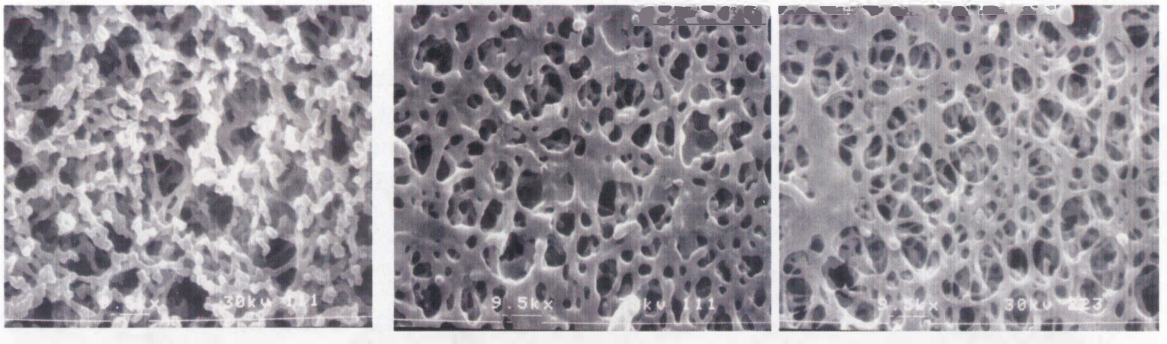

Figure 11. SEM Images of GSWP (MF-HPI) Membrane (from the left: clean and filtered with Bultière Reservoir and Yffiniac River; magnification : 9500X)

Contact Angle. Contact angle is used to investigate the hydrophobicity/hydrophilicity of a membrane surface (Table 6). It measures the angle of a water drop on the membrane surface by a goniometer. While it is not a very accurate measurement, it is still informative to explain the relative changes of a membrane property by fouling. The contact angle of the clean hydrophilic membranes was less than 20° while the contact angle of the clean hydrophobic membranes was greater than 50°. As a membrane is more hydrophobic, the contact angle will be higher. After filtration, the contact angle (hydrophobicity) was increased for hydrophilic membranes and was decreased for hydrophobic membranes, reflecting the nature of the foulant.

Table 6. Contact Angle (degrees) of Each Membrane

		Clean	Marne	Cazau	Bultière	Yffiniac
MF	HPI (GSWP)	19	40	20	27	23
	HPO (GVHP)	83	66	45	79	75
UF	HPI (YM100)	18	41	33	23	32
	HPO (PES100)	58	30	44	47	44

3.2.3 Modeling

Flux decline data for bulk natural waters were modeled to help explain fouling propensity within the context of a mathematical equation. An empirical model was employed to evaluate correlation of experimental flux decline results. The equation presented in Equation 1 is governed by three parameters; k_a, k_b and k_c. The constant k_a is a dimensionless constant that is representative of a *total*, immediate short-term flux-decline potential by NOM, k_b (time^{-1}) represents a *rate* of short-term flux decline, and k_c (time^{-1}) reflects long term flux decline kinetics (related to either or both gradual pore plugging due to adsorption or layer (cake) buildup on the surface).

$$\frac{J_t}{J_o} = \frac{1}{1 + k_a\left(1 - e^{-k_b t}\right) + k_c t} \qquad 1.1$$

Table 7 provides k_a, k_b, and k_c values obtained with non-linear estimation by a software package (Excel-Solver). The three model parameters were evaluated based on both time (min, t = time) and delivered DOC (mg/m^2, t = delivered DOC) versus J/Jo. Figure 12 illustrates comparisons between experimental results of flux decline and model predictions. Overall, the data were well fit by the model.

An attempt was made to develop multiple regression models to predict the constants, k_a, k_b, and k_c, as a function of feed water characteristics and membrane properties. Both linear and non-linear regression was attempted but with little success, suggesting that a statistical interpretation of model constants is inadequate and further attempts should be based on the physics of the system.

Table 7. Empirical Flux Decline Model Fitting Parameters

Time Based					
Source	Membrane	J/J_0 (1hr)	k_a	k_b	k_c
Marne River	YM100	48%	0.2961	0.0708	0.0362
	PES	16%	0.1144	0.0814	0.0107
	GSWP	65%	5.5686	-0.0067	-0.0138
	GVHP	47%	0.2168	0.0987	0.0499
Cazau Lake	YM100	55%	0.5982	0.0501	0.0201
	PES	28%	0.1622	0.0980	0.0245
	GSWP	67%	0.2618	0.0538	0.1136
	GVHP	73%	2.5339	0.0700	0.0012
Bultière Reservoir	YM100	32%	0.6800	0.0163	0.0003
	PES	21%	0.2347	1.0549	0.0019
	GSWP	60%	0.2335	0.1327	0.0903
	GVHP	56%	0.2589	0.2334	0.0630
Yffiniac River	YM100	32%	0.0508	0.0973	0.1296
	PES	46%	0.0691	2.069	0.1523
	GSWP	64%	0.3073	0.1159	0.0758
	GVHP	69%	0.6517	0.1291	0.0420
Delivered DOC Based					
Source	Membrane	J/J_0 ($\approx$250mg/m^2)	k_a	k_b	k_c
Marne River	YM100	41%	0.2142	0.0079	0.0102
	PES	16%	0.1188	0.0160	0.0022
	GSWP	22%	0.1332	8.2E-10	0.0090
	GVHP	41%	0.1381	0.0135	0.0159
Cazau Lake	YM100	37%	0.4028	0.0026	0.0043
	PES	14%	0.1530	0.0043	0.0014
	GSWP	17%	0.1711	1.9E-09	0.0049
	GVHP	71%	62.3608	0.0008	-0.0006
Bultière Reservoir	YM100	15%	0.4462	0.0012	0.0007
	PES	20%	0.2346	0.0624	0.0001
	GSWP	12%	0.0326	0.0093	0.0110
	GVHP	40%	0.1797	0.0261	0.0137
Yffiniac River	YM100	11%	0.0045	0.0179	0.0962
	PES	12%	0.0544	2.4E-09	0.0136
	GSWP	7%	0.0527	0.0012	0.0061
	GVHP	42%	0.3804	0.0037	0.0048

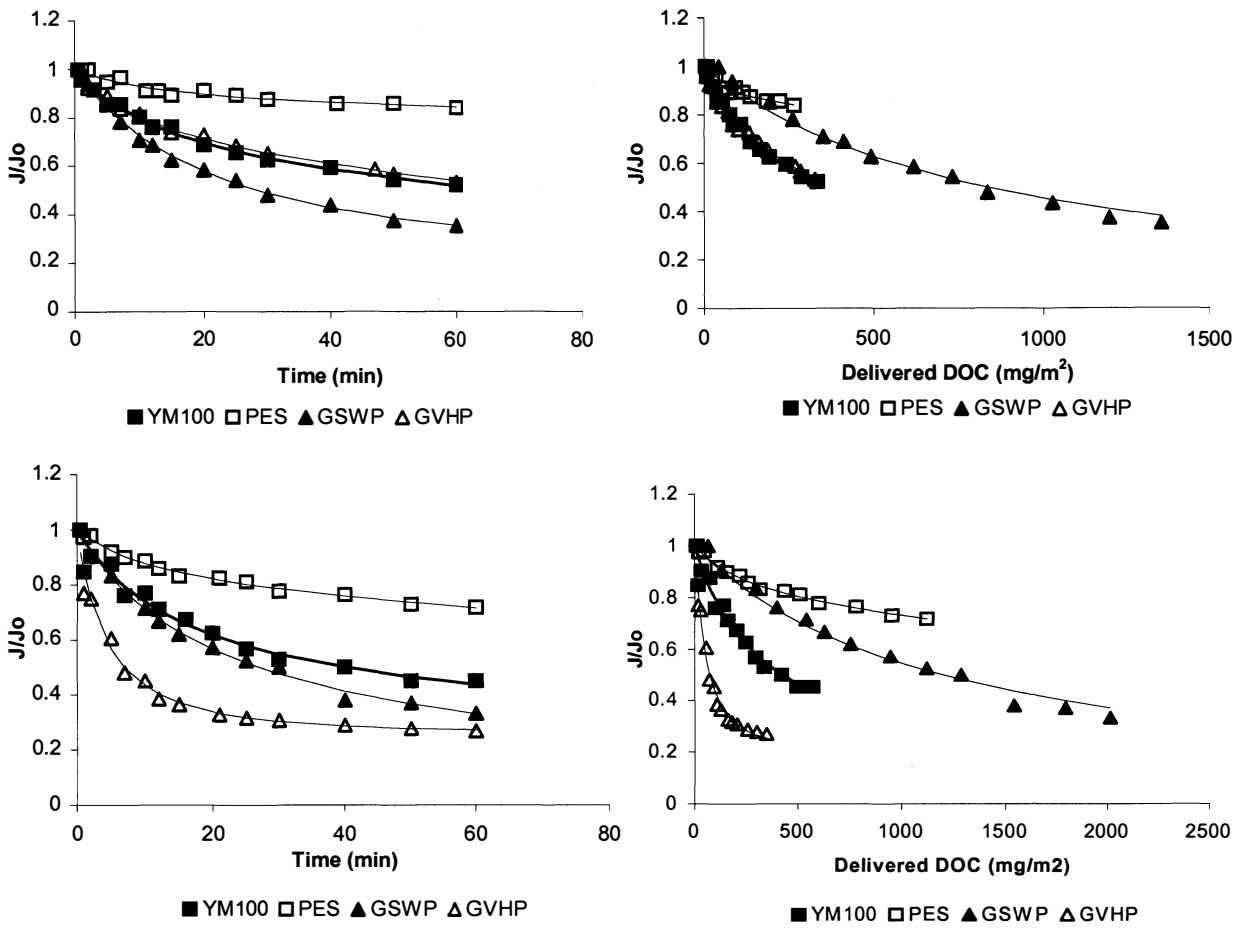

Figure 12. Comparisons between experimental flux decline results (dots) and model predictions (lines) (upper: Marne River, lower: Cazau Lake)

3.2.4 Summary

Natural waters with a high content of hydrophilic (HPI) fraction resulted in more significant flux decline. This may due to this fraction containing colloidal and/or macromolecular organic matter with hydrophilic and non-humic properties. Distinctive differences in flux decline between hydrophobic and hydrophilic membranes were not observed suggesting that other membrane properties may be more influential. The size and steric conformation of molecules and roughness of membranes are likely important influential factors in affecting flux decline.

From SEC-DOC/UV analyses, the first peaks are reduced effectively during most of the membrane filtrations due to their large molecular weight. These large molecular weight peaks correspond to macromolecular compounds and/or colloidal organic matter, and contribute to significant organic matter fouling during low pressure membrane filtration.

From the morphological analyses, significant fouling was caused by adsorption of NOM around membrane pores by smaller molecules and/or pore blockage by larger molecules and/or colloids. Backwashing experiments also support the notion that the fouling of UF membranes is more likely affected by cake layer formation while MF membrane is more attributed to pore blockage.

Ranking of Membranes. From this work, the fouling potential of the various membranes can be listed below, ordered from highest to lowest, for the four membranes and the four feed waters:

Marne:	HPO-MF ~ HPI-UF > HPI-MF > HPO-UF
Cazau:	HPO-MF > HPI-UF > HPI-MF > HPO-UF
Bultière:	HPO-MF > HPI-MF ~ HPI-UF ~ HPO-UF
Yffinac;	HPO-MF > HPO-UF > HPI-MF > HPI-UF
Overall:	HPO-MF > HPI-MF ~ HPI-UF > HPO-UF

The membrane property trends were as follows:

Roughness (Qualitative):	HPO-MF ~ HPI-MF > HPI-UF ~ HPO-UF
Hydrophobicity:	HPO-MF > HPO-UF > HPI-MF ~ HPI-UF
Surface Charge (Negative):	HPO-UF > HPO-MF > HPI-UF > HPI-MF

These results indicate that MF membranes are more prone to fouling than UF membranes. Trends according to membrane hydrophobicity/hydrophilicity are less clear, likely because surface roughness is a more influential factor than HPO/HPI character. Based on AFM, the two MF membranes exhibited greater surface roughness than the two UF membranes. An interesting aspect of the HPO-UF is its highest surface charge, a property that might offset its hydrophobicity. In recognition that productivity is influenced by both flux and fouling, it is noteworthy that the PWPs of the membranes follow the order: HPI-MF > HPO-MF > HPI-UF > HPO-UF.

Ranking of Feed Waters. The fouling potential of the various source (feed) waters, based on flux decline as a function of delivered DOC, is listed below, ordered from highest to lowest, for the four source waters and the four membranes:

HPO-UF:	Bultière > Cazau ~ Yffinac ~ Marne
HPI-UF:	Cazau ~ Marne > Bultière > Yffinac
HPI-MF:	Cazau ~ Marne > Bultière ~ Yffinac
HPO-MF:	Cazau > Bultière > Yffiniac ~ Marne
Overall:	Cazau > Marne ~ Bultière > Yffinac

Water quality parameter trends are summarized in terms of SUVA (ranked from low to high), percent of the DOC represented by the hydrophilic (HPI) fraction (ranked from high to low), and the magnitude of the macromolecule/colloid component as represented by the size of the high-MW SEC peak (ranked from high to low):

SUVA:	Cazau < Marne < Bultière < Yffinac
HPI Fraction:	Cazau > Bultière > Marne > Yffinac
High MW SEC Peak:	Cazau > Bultière > Marne ~ Yffinac

These NOM attributes; low SUVA, high HPI fraction, and high MW peak; are the signature of algal organic matter (AOM) and wastewater effluent organic matter (EfOM) (Her, 2002, Jarusutthirak, 2002). Thus, it is likely that the most problematic sources are impacted by algae, or possibly wastewater effluent.

Modeling. The flux decline model represents a potential basis for a new flux decline "index" in which the constants; k_a, k_b, and k_c, capture kinetic based fouling trends. Such an approach involves probing potential correlations between each of the constants versus membrane and/or source (feed) water characteristics. However, attempts to develop statistically based predictions of model constants were unsuccessful.

3.3 Organic Matter Isolates/Fractions

In this section, we present a focused analysis of detailed measurements done with two natural water sources: one that was affected by an algal bloom and the other was dominated by allochthonous NOM. From the filtration of two natural waters and their isolates/fractions, foulants and fouling mechanisms were identified with organic matter (OM) analyses being proposed as surrogate tests for fouling potential.

In the previous section, we presented detailed studies of NOM fouling in low pressure (MF and UF) membranes with four different natural waters. We also presented initial, empirical, quantitative parameters to describe the dead-end filtration results, with the aim of correlations with the surrogate analytical measurements of the water and the membrane properties. In this section, we present results of a statistical correlation matrix used as a guide in the next iteration of the modeling.

3.3.1 Materials and Methods

Membranes and Filtration Apparatus. Four different membranes were used in (constant pressure) flux decline tests for the study of NOM fouling (see Table 1); two MF and two UF membranes possessing hydrophilic (HPI) or hydrophobic (HPO) properties.

Composition (Water Quality) of Source (Feed) Waters. A French source water, Brittany Reservoir, and a USA source water, Silver Lake, were selected as an autochthonous source taken during an algal bloom and an allochthonous source, respectively. The Brittany Reservoir is a eutrophic reservoir with periodic algal blooms and dominated by autochthonous NOM, while Silver Lake is a high elevation lake dominated by allochthonous NOM derived from terrestrial runoff. The water quality of the two water sources are tabulated in Table 8 and the % of DOC profile by XAD-8/4 fractionation is displayed Table 9. The Brittany water shows a very high DOC content of the hydrophilic (HPI) fraction.

Table 8. General Water Quality of Source (Feed) Waters*

Source	Brittany Reservoir	Silver Lake
DOC (mg/L)	8.99	2.39
UVA_{254} (cm^{-1})	0.21	0.073
SUVA (L/mg·m)	2.34	3.1
pH	7.3	6.94
Conductivity (μs/cm)	393	29
Ca^{2+} (mg/L)	23.7	3.22
Fe (mg/L)	≤ MDL**	0.02
Si (mg/L)	2.0	2.55

*After 0.45μm pre-filtration
**MDL: method detection limit (Fe: 0.002ppm)

Table 9. XAD-8/-4 Fractionation of Source (Feed) Waters

Source Water	Hydrophobic DOC (%)	Transphilic DOC (%)	Hydrophilic DOC (%)
Brittany Reservoir	24	26.5	49.5
Silver Lake	37	25	38

From both sources, NOM isolate/fractions were obtained by the general procedure adapted from Leenheer and Aiken (Aiken, 1988, Thurman et al., 1978, Aiken and Leenheer, 1993, Aiken et al., 1992, Aiken et al., 1979). The isolates include organic colloids, the hydrophobic (HPO) fraction, and the transphilic (TPI) fraction. Isolation of the HPI fraction (after colloid removal) was omitted due to its very small amount relative to the other fractions (~5% of DOC) and the difficulty of isolation. It is noteworthy that, if colloids are not pre-isolated, they end up in the HPI fraction and then this fraction becomes much larger. It is important to recognize that the HPO and TPI fractions consist of HPO and TPI acids. For further analytical measurements with similar foulants, some known macromolecules such as dextran (a representative polysaccharide) and albumin (a representative protein), and Klamath Lake algal organic matter (AOM) were also tested. Feed waters were prepared with NOM isolates dissolved into Milli-Q water with a DOC concentration of about 5mg/L and adjusted to neutral pH. Feed waters were 0.45μm pre-filtered to investigate the behavior of dissolved organic matter (DOM) on membrane fouling.

3.3.2 Characterization of NOM and Membranes

High Pressure Size Exclusion Chromatography. Molecular weight (MW) distributions were determined by a High Pressure Size Exclusion Chromatography (HP-SEC) method. A high performance liquid chromatograph (HPLC, LC600 Shimadzu) was used with UVA (SPD-6A Shimadzu) and on-line DOC detectors (modified Sievers Turbo Total Organic Carbon Analyzer) following size separation by a HW-50S or HW-65S column. The column packing material is a Toyopearl resin, semi-rigid, spherical beads

with a hydrophilic surface that are synthesized by co-polymerization of ethylene glycol and methacrylate-type polymers (GROM, Denmark). The separation capacity of the HW-50S column (the first column) is 500 ~ 20000 dalton based on dextrans, and 500 ~ 80000 dalton with globular proteins. The separation capacity of the HW-65S column (the second column) is 10000~1000000 dalton with dextrans and 40000~5000000 dalton with globular proteins. The DOC detector is connected to the UVA detector waste line sequentially. UVA and DOC data are recorded every 6 seconds by a modified Labview software. The SEC column separates compounds based on hydrodynamic molecular size. The average retention time is affected by the effective size and structure of the molecules. Consequently, larger and linear shaped molecules are excluded earlier than smaller and globular shape molecules. Polyethylene glycols (PEGs) were used for calibration of the relationship between MW and retention time (Her et al., 2002, Lee, 2003).

3D Fluorescence Excitation Emission Matrix Spectrometry. A JY-Horiba/Spex Fluoromax-2 fluorometer with a xenon lamp as an excitation source was used for measuring 3D-EEM spectra of NOM sources (Jobin-Yvon-Horiba, Edison, NJ). 3D-EEM spectra were obtained by collecting excitation and emission spectra over a range (200 ~ 500nm). Data were analyzed with DataMax software and displayed by contour lines. Spectral subtraction was performed to remove blank spectra mainly caused by Raman scattering.

Attenuated Total Reflection-Fourier Transform Infrared Spectroscopy. ATR-FTIR provides information related to the presence of specific functional groups of various isolates and the membrane surface. The adsorption spectrum was obtained with a Nicolect Magna-IR 750 series II FTIR spectroscopy (Nicolet, Madison, WI). A KBr pellet was used for solid samples and an ATR accessory with ZnSe crystal was used for membrane specimens. The measured wavelength was between 4,000 and 400 cm^{-1}.

Atomic Force Microscopy and Scanning Electronic Microscopy. The AFM employed is made by Digital Instruments, Inc., and the data were analyzed using their Nanoscope II software. The tip size was 4~10nm and was made of an etched single crystal silicon. Given the pore size of the candidate membrane, the tip would be expected to recognize MF (220 nm) pore but not necessarily UF pores. Clean membrane specimens were prepared with MQ water filtration and dried at room temperature to obtain an actual surface, and fouled membrane specimens were dried at room temperature. While the drying procedure may cause a slight distortion of the membrane surface, the morphology was compared to a dried clean membrane, side by side, providing a qualitative and semi-quantitative comparison. A sample specimen was fixed on a glass slide and was scanned with scan sizes of 10 × 10 μm for MF and 5 × 5 μm for UF membranes.

For SEM analysis, MQ filtered clean membranes and fouled membranes were completely dried at room temperature. A sample specimen was mounted with graphite adhesive and coated with gold (Au) on a carbon coated aluminum stub and examined at 30 kV accelerating voltage (ISI-SX-30, Topcon America corporation) for SEM analyses.

3.3.3 Results and Discussion

The two different water sources were filtered with the four different types of membranes. As illustrated in Figure 13, Brittany Reservoir showed greater flux decline (up to 83% decline at 60 minutes filtration time and up to 64% decline at 200mg/m^2 delivered DOC) than Silver Lake (57% and 55%, respectively) in each set of membrane filtrations. The overall % flux decline is shown in Table 10. MF membrane filtration exhibited greater flux decline than UF membrane filtration due to different fouling mechanisms. The flux decline of MF membranes was attributed to pore blockage and/or pore constriction, and that of UF membranes was attributed to surface coverage. Complete loss (of availability to filtration) of open pores yields much a faster kinetics of (steeper) flux decline.

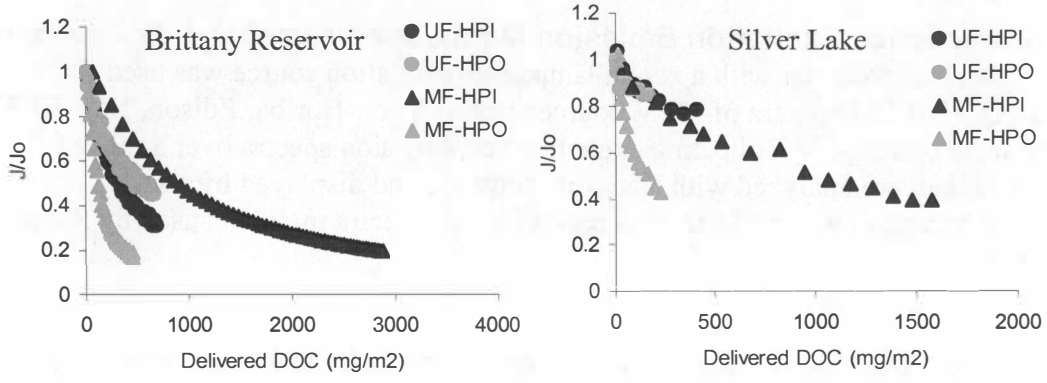

Figure 13. Flux Decline Tests with Different Source Waters.

NOM fractions, isolated in the form of colloids (by dialysis (3,500 dalton)) and a hydrophobic (HPO) fraction (by XAD-8 resin adsorption) from the source waters, were membrane-filtered in the same manner. The HPO fraction generally corresponds to ~50% of the DOC in natural waters. However, Figure 14 indicates that colloid fraction showed significantly more flux decline than the HPO fraction. The Brittany colloids caused similar or greater flux decline than Silver Lake colloids; the greater flux decline may be attributed to the algal organic matter associated with the Brittany source.

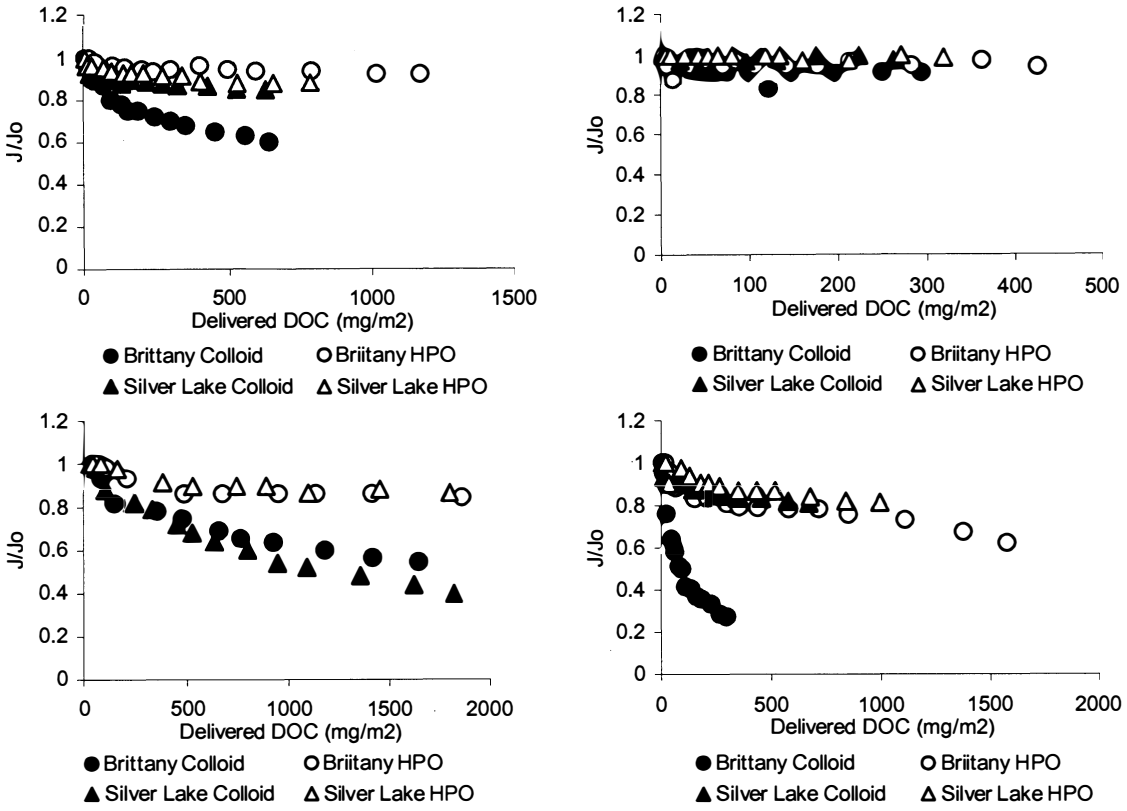

Figure 14. Flux Decline with Different Isolates in Membrane Filtration (upper left UF-HPI, upper right UF-HPO, lower left MF-HPI, lower right MF-HPO)

Figure 15 presents the SEC-DOC results for the Brittany water. The organic colloids showed a high DOC response in a high molecular weight region with a relatively low response of UV. This region of the SEC chromatograms corresponds to macromolecular compounds such as polysaccharides and proteins, which also exist in a colloidal form, and are deemed to be responsible for significant fouling of the low pressure membranes.

Table 10. Flux Decline of Source (Feed) Waters

Membrane		Brittany Reservoir	Silver Lake
YM100 (UF-HPI)	Time (60min)	69% (≈687mg/m^2)	21% (≈412mg/m^2)
	Delivered DOC (≈200mg/m^2)	**37%** (11min)	**17%** (30min)
PES (UF-HPO)	Time (60min)	54% (≈663mg/m^2)	15% (≈167mg/m^2)
	Delivered DOC (≈200mg/m^2)	**31%** (14min)	**15%** (60min)
GSWP (MF-HPI)	Time (60min)	80% (≈2880mg/m^2)	42% (≈1569mg/m^2)
	Delivered DOC (≈200mg/m^2)	**15%** (2min)	**18%** (5min)
GVHP (MF-HPO)	Time (60min)	83% (≈460mg/m^2)	57% (≈230mg/m^2)
	Delivered DOC (≈200mg/m^2)	**64%** (16min)	**55%** (50min)

Figure 16 compares SEC-DOC/UV responses between feed and permeates with the four different types of membranes. The high responses of the first peak were dramatically reduced while the second peaks corresponding to humic substances were not effectively removed. Thus, the significant flux decline in Brittany water was caused by these types of molecules (i.e. colloids and macromolecules); it is noteworthy that these molecules end up in the HPI fraction without pre-isolation of colloidal organic matter. This is reflected in the result of the XAD –8/-4 resin fractionation providing a high content of the hydrophilic fraction. In comparison between MF/UF-HPO and MF/UF-HPI membranes, it is appears that hydrophobic membrane exhibits better removal of high molecular weight compounds.

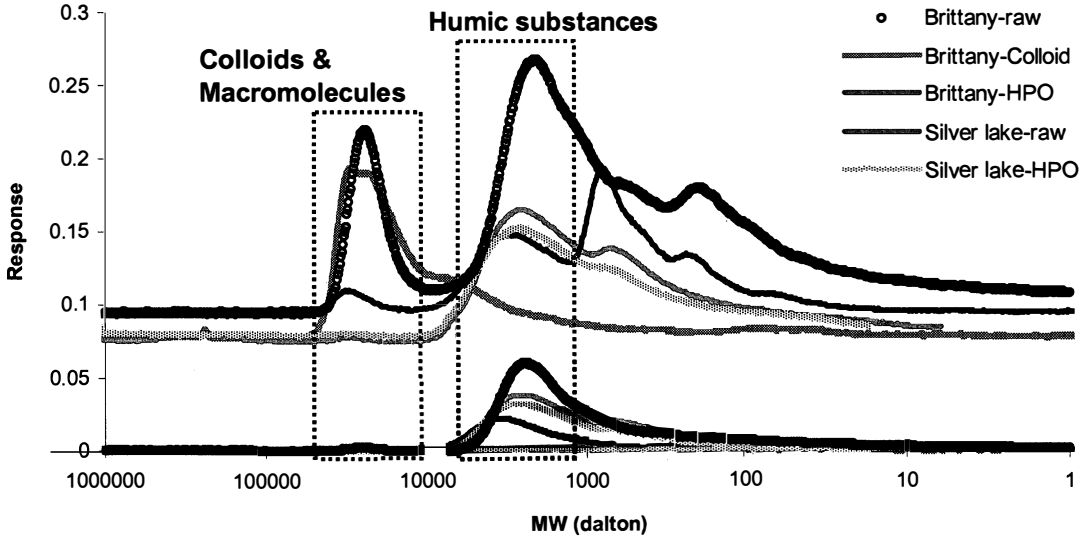

Figure 15. SEC-DOC/UV analysis of raw waters and isolates

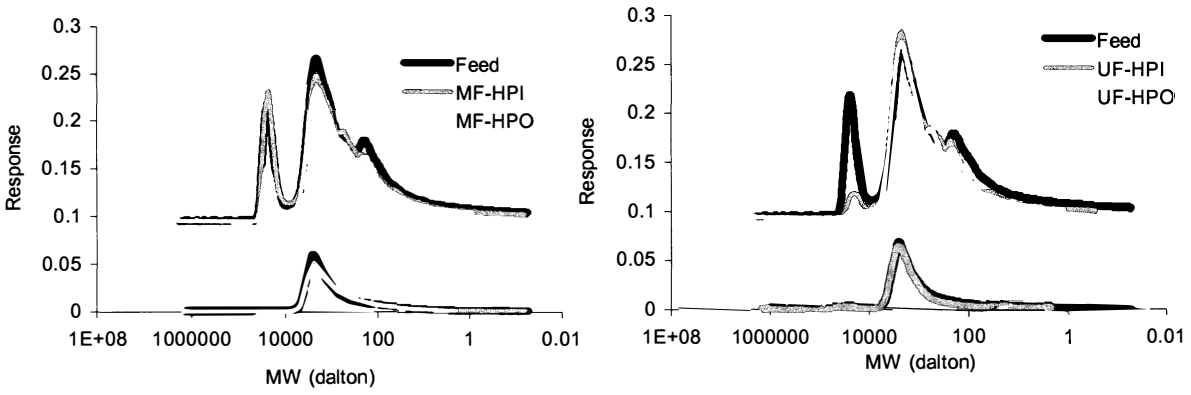

Figure 16. Comparison of SEC-DOC/UV analysis between Brittany (raw) water and permeate waters after membrane filtration

FTIR analysis in Figure 17 also suggests a signature of macromolecules represented as foulants. Three characteristic IR peaks of Brittany colloids and Klamath AOM (1653 cm^{-1}, 1543 cm^{-1}, and 1074 cm^{-1}) are overlapped and distinctively different from the other two isolates. The C=O stretching (amide I band) of primary amides has a strong peak in the region of 1650 cm^{-1} and that of secondary amides absorbs near 1640 cm^{-1}. N-H bending (amide II band) of secondary acyclic amides displays in the region of 1570-1515 cm^{-1} and results from interaction between the N-H bending and the C-N stretching of the C-N-H group (Silverstein and Webster, 1998). Thus, the first two peaks are characteristic of a peptide bond. A peptide bond joins amino acids with an amide linkage in a protein, and is very planar and very rigid (Figure 17). The peak at 1074 cm^{-1} is C-O stretching and the peaks at 3437 cm^{-1} is O-H stretching come from alcohols associated with polysaccharides, usually appearing in the region of 1260-1000 cm^{-1} and in the region of 3200-3550 cm^{-1}, respectively. Generally, the OH stretching vibrations of the SiOH group shows up in the same region as the alcohols, i.e., 3700-3200 cm^{-1} and Si-O bands are at 830-1110 cm^{-1}. However, the peaks of the organic colloid fraction presumably came from alcohols because of pretreatment with hydrofluoric acid to eliminate the SiO_2 influence during the colloid isolation; moreover the bulk water exhibited low Si. The peak at 1716 cm^{-1} in the HPO and TPI fractions is responsible for C=O stretching and the peak at 2925 cm^{-1} corresponds to O-H stretching in a dimeric carboxylic acid. Thus, the results suggest that two types of compounds, proteins and polysaccharides, may impart significant fouling of low pressure membranes.

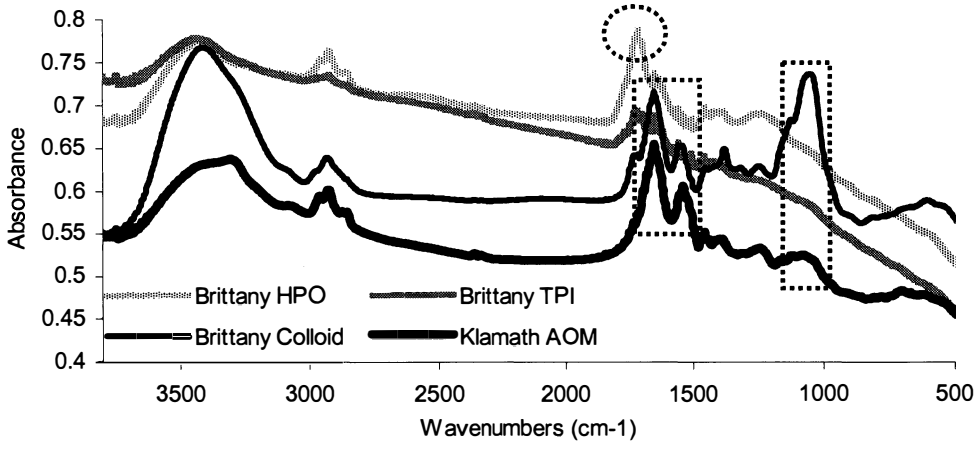

Figure 17. FTIR Analysis of different source of isolates

Figures 18 and 19 illustrate 3-D fluorescence EEM (excitation-emission matrices) of various NOM isolates/fractions, the AOM, and model compounds. As a general rule, humic-like OM exhibits a peak(s) at higher Ex/Em wavelengths while protein-like OM shows a peak(s) at lower Ex/Em wavelengths. The Brittany HPO shows a maximum at an excitation (Ex) of 334 nm and an emission (Em) of 434 nm; the Brittany colloids show a very different maximum peak at Ex = 278 nm and Em = 304 nm. The Brittany TPI exhibits maxima at both peaks due to its both humic and non-humic content. Proteins show a maximum at Ex ~280 nm and Em ~336 nm. The Klamath AOM shows maxima at four peaks: Ex = 355 nm and Em = 436 nm, Ex = 279 nm and Em = 445 nm, Ex = 282 nm and Em = 338 nm, and a very weak intensity at Ex = 278 nm and Em = 304 nm, demonstrating that Klamath AOM contains both humic-like substances and protein-like substances. The fluorescence EEM technique does not recognize polysaccharide-like material because of the absence of fluorophores in the molecule.

The filtration of colloids caused high flux decline; the colloids also indicated a content of protein-like substances. Thus, the protein-like substances can be attributable to significant fouling in low pressure membrane filtration, and significant fouling potential can be inferred by a peak intensity of EEM at Ex = ±280 nm and Em = 300-350 nm.

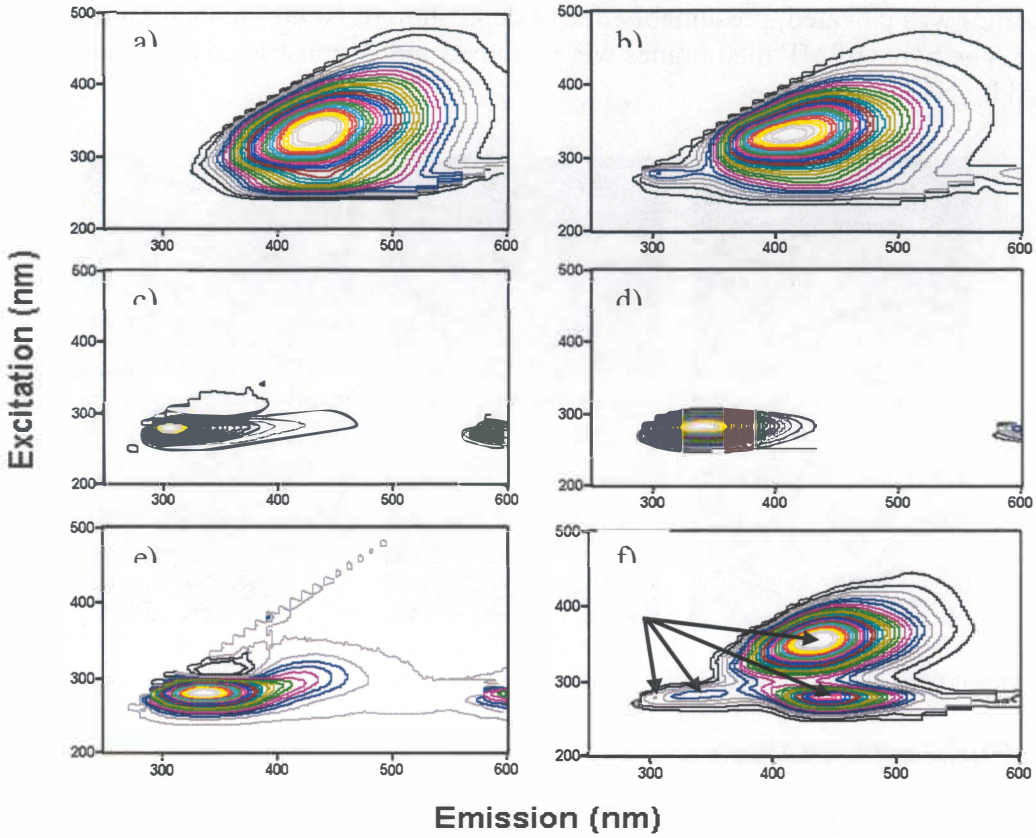

Figure 18. Fluorescence Contour Maps of Isolates/Fractions and Organic Compounds (a: Brittany HPO, b: Brittany TPI, c: Brittany Colloid, d: BSA, e: γ-globulin, f: Klamath AOM).

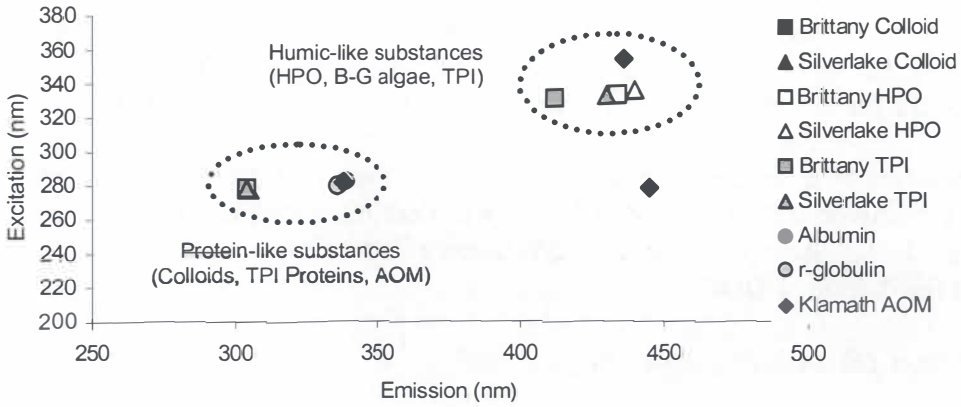

Figure 19. EEM of Various Isolates/Fractions and Organic Compounds.

The AFM measurements (Figure 20) indicated that the surface topography of fouled UF membranes was elevated, presumably due to deposition of NOM on the membrane surface. The pores of MF membranes were reduced and/or constricted and presumably blocked by NOM aggregates.

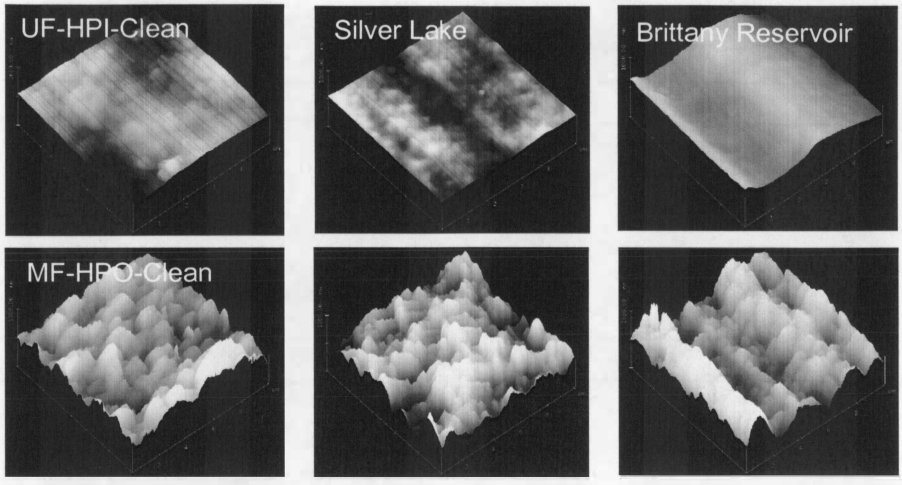

Figure 20. Morphological Differences between Clean and Fouled Membranes

3.3.3 Modeling Flux Decline

Correlation Matrix. The following tables provide the Pearson's correlation matrix among variables derived from the water quality measurements, the membrane properties, and the parameters from the empirical fit of the flux decline based on delivered DOC.

A strictly empirical model was used to provide a simple mathematical form to capture the three main characteristics of differential flux decline: 1) a very quick initial drop in permeation rate, 2) an exponential decay, 3) and a continuous decline over time. Modeling was performed to provide more flexible (and hopefully predictive) quantitative figures-of-merit to try to correlate with the surrogate tests for fouling propensity. The empirical flux-decline equation uses three parameters; k_a, k_b and k_c representing, respectively, the immediate total, short term flux-decline potential by pore blockage; the time constant for this short term potential; and the time constant for long term, continuous flux decline due to cake/gel layer growth or gradual pore radius diminuation. The parameters were evaluated based on both time (min, t = time) and delivered DOC (mg/m^2, t = delivered DOC) fitted to J/J_0. It was demonstrated that the model could well fit the flux decline data points. In the correlation effort below we simply used the values based on the delivered DOC.

Empirical modeling equation:

$$\frac{J_t}{J_o} = \frac{1}{1 + k_a\left(1 - e^{-k_b t}\right) + k_c t}$$

The Pearson's correlation reflects the degree of linear relationship between two variables in each set. It was determined using STATISTICA software (Starsoft Inc., OK). The coefficients range from +1 to -1. A correlation of +1 means that there is a perfect positive linear relationship between variables, while -1.00 shows a perfect negative relationship. The smallest correlation is zero.

As the first comparison, Table 11 addresses the correlation within internal groups. First, within the water quality parameters DOC versus UV254, DOC versus HPI fraction and UV254 versus SUVA have very high relationships (up to 0.93). The high molecular mass (HW) peak has it closest linear correlation with SUVA, that is, the higher the SUVA, the lower the HW peak. But the correlation is not well-represented by a linear relationship, which is why the SEC or fluorescence analysis is needed.

The next internal correlation is among the membrane parameters. MWCO versus roughness (this may simply be an artifact of the two MF membranes being more rough than the two UF membranes that were more smooth) and contact angle versus zeta potential have a higher (up to 0.99) correlation than any other variables. This latter result bears further scrutiny. Permeability has relatively high relationships with all of membrane properties.

Table 11. Pearson's Correlation Matrix: Water Quality Parameters and Membrane Properties

Water Quality Parameters						
No.	Variables	DOC	UV254	SUVA	HPI Fraction	HW peak
1	DOC	1	0.9284	0.7399	0.9023	0.1640
2	UV254		1	0.931	0.6820	-0.1931
3	SUVA			1	0.4074	-0.5372
4	HPI Fraction					0.5032
5	HW peak					1
Membrane Properties						
No.	Variables	MWCO	Roughness	Contact Angle	Zeta Potential	Permeability
6	MWCO	1	0.9895	0.3338	0.6506	0.7068
7	Roughness		1	0.4268	0.7347	0.7236
8	Contact Angle			1	0.9203	0.8057
9	Zeta Potential				1	0.8582
10	Permeability					1

Table 12 presents the correlation matrix between the fitting parameters and both water quality and membrane properties. Most importantly, there is no strong linear correlation between any of the parameters. This implies that one must become more mechanistic in deciding how to combine membrane and water properties to correlate with flux decline parameters. Having said that, we do see some clusters of variables that seem to be the most highly related to the flux decline parameters.

Attempts to develop multiple regression models to predict the model constants as a function of various feed water characteristics and membrane properties were unsuccessful based on both linear and non-linear regression techniques.

Table 12. Pearson's Correlation Matrix: Flux Decline Constants

Variable	J/J_0	k_a	k_b	k_c
DOC	-0.3128	-0.0875	0.3202	0.0415
UV254	-0.3643	-0.2142	0.3730	0.1761
SUVA	-0.3810	-0.3367	0.3905	0.3105
HPI Fraction	-0.2123	0.0445	0.2174	-0.0919
HW peak	0.1767	0.4021	-0.1819	-0.4206
MWCO	0.3197	0.2544	-0.3583	-0.2112
roughness	0.3320	0.2440	-0.4317	-0.1943
contact angle	-0.3141	-0.1974	-0.4907	0.1819
zeta potential	-0.0393	-0.0258	-0.5781	0.0445
permeability	-0.2646	-0.0839	-0.3589	0.0584

3.3.4 Summary

Brittany reservoir water has a higher content of algal organic matter and provided significant flux decline, and colloids isolated from an algal impacted (authochthonous) source showed more significant flux decline than colloids isolated from an allochthonous source. In SEC, colloids showed a high DOC response in a high molecular weight region with a relatively low response of UV. This region of the SEC chromatograms corresponds to macromolecular compounds such as polysaccharides and proteins, which may also exist in a colloidal form. 3-D EEM and FTIR analysis revealed the content of protein-like substances in colloids and AOM, supporting the notion of protein-like substances in each NOM source. Conclusively, both organic colloids as well as intercellular and/or extracellular algal organic matter in the forms of protein or polysaccharide-like substances may be responsible for significant membrane fouling. From the morphological analyses, the elevation of UF membrane surface topography is presumably due to deposition of NOM on the membrane surface. The pores of MF membranes were reduced and presumably blocked by NOM aggregates.

An empirical flux decline model was able to capture flux decline trends but attempts to relate model constants to feed water characteristics and membrane properties proved unsuccessful.

4. Part II: Identification of Organic Foulants and Fouling Mechanisms in High Pressure (NF/RO) Membranes

4.1 Introduction

The work reported in this part of the report is intended to extend the work reported in the previous part from low pressure to high pressure membranes, both nanofiltration (NF) and reverse osmosis (RO) membranes. In this part, two work efforts will be reported in separate sections, highlighting wastewater effluent organic matter (EfOM) and algal organic matter (AOM), respectively.

4.2 Effluent Organic Matter

4.2.1 Isolation and Characterization of EfOM Isolates

EfOM fractions were isolated from bulk EfOM associated with wastewater effluent from two French wastewater treatment plants. The fractionation method utilized vacuum (rotary) evaporation to concentrate a wastewater secondary effluent sample, and 3500-dalton dialysis membrane to separate colloidal EfOM before non-ionic resins were used to isolate additional fractions. After isolation of EfOM colloids, XAD-8 and XAD-4 resins were then employed to fractionate hydrophobic and transphilic fractions, respectively. The hydrophilic fraction, passing through the XAD-4 column, contains salts. In this study, the low molecular weight hydrophilic (HPI) fraction was not further considered. In previous work without the dialysis step, hydrophilic colloids and macromolecules were part of the HPI fraction, making it appear to be the most problematic fraction in EfOM-related fouling. Thus, with this present approach, the EfOM was fractionated into three different fractions, including colloidal (COL), hydrophobic (HPO), and transphilic (TPI) EfOM. The functionally distinct DOC fractions were characterized by several of the analytical methods discussed in the previous part of the report including Fourier transform infrared (FTIR) spectroscopy, size exclusive chromatography (SEC) with on-line UVA and DOC detectors, and specific UVA (SUVA); additionally, total sugar determinations were made. Figures 21 and 22 exhibit SEC chromatograms of EfOM isolates from Saint Julien l'Ars secondary effluent (ST-SE) and Naintrè secondary effluent (NA-SE), respectively. The SEC results show that colloidal EfOM primarily consists of large molecular weight compounds with a hydrophilic character. The HPO and TPI fractions represented the characteristics of humic and fulvic acids with a high UV response. However, the TPI fraction exhibited a smaller molecular size and more hydrophilic character than the HPO fraction. Figure 23a and 23b represent a correlation of UVA254 and DOC and of polysaccharides and DOC, respectively, for each fraction. The results indicated that the HPO fraction possessed a higher SUVA, an index of aromaticity, than the TPI fraction, whereas colloids contained

more polysaccharides than the TPI and HPO fractions. These results are consistent with the SEC data.

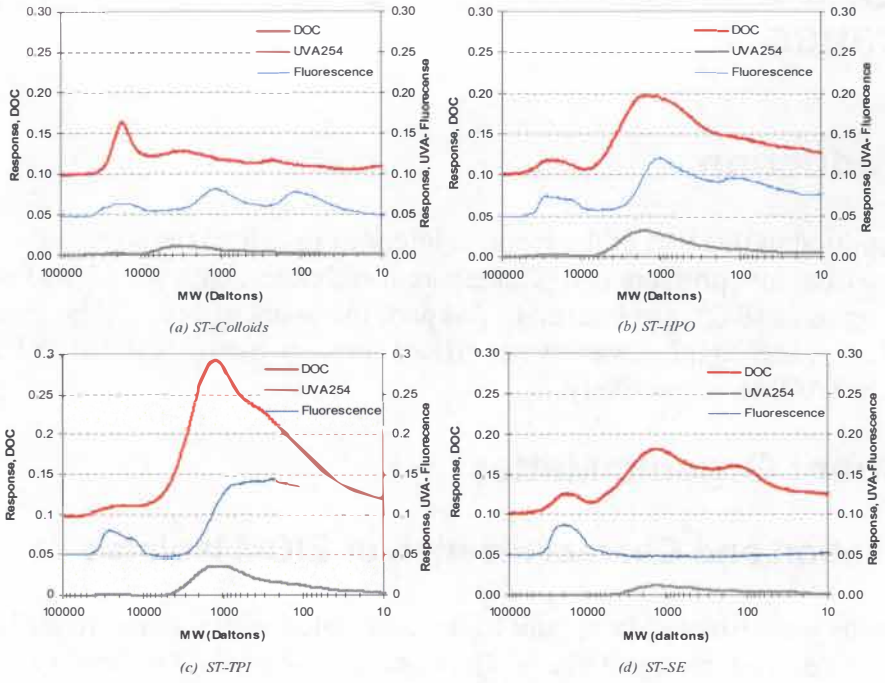

Figure 21. SEC chromatograms of ST-isolates and associated ST-SE bulk water

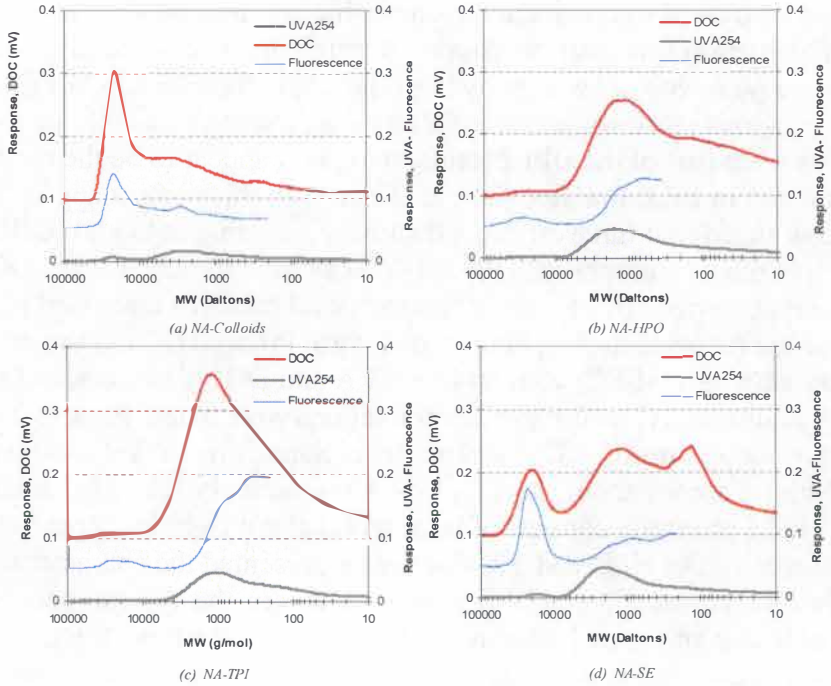

Figure 22. SEC chromatograms of NA-isolates and associated NA-SE bulk water.

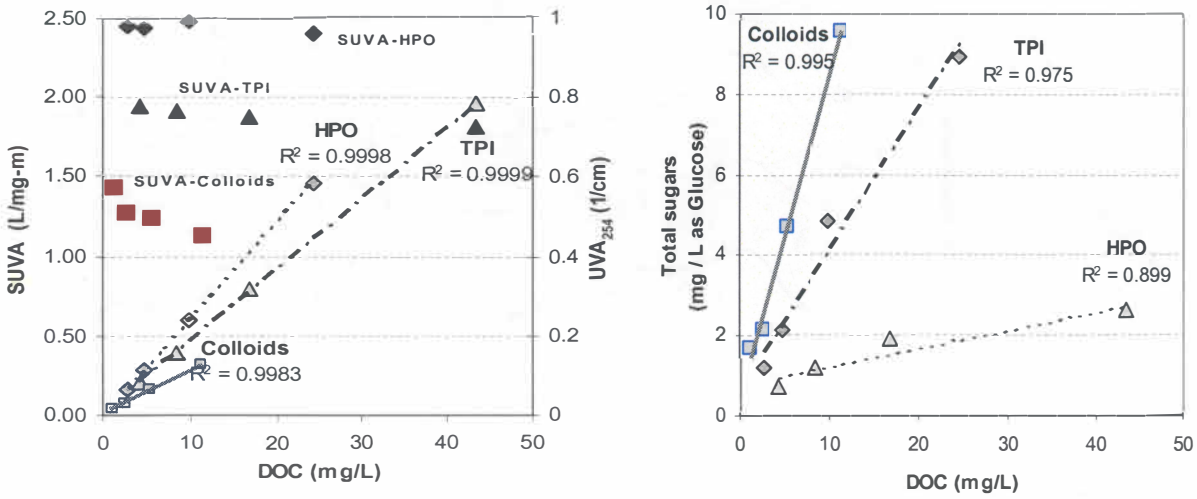

(a) DOC vs UVA_{254} and SUVA **(b) DOC vs total sugars**

Figure 23. Correlation of DOC vs (a) UVA_{254} and SUVA (b) total sugars

FTIR spectra of EfOM isolates from ST-SE and NA-SE are shown in Figures 24 and 25, respectively. As found in the colloidal fraction, the peaks at wave numbers of 1540 and 1640 cm^{-1} reflect functional groups of primary and secondary amides, indicative of proteins. A broad peak at 1040 cm^{-1} and an OH broad peak at 3400 cm^{-1} indicate alcoholic groups associated with polysaccharides. The overall FTIR results of colloidal fractions indicate that the major components of colloids are polysaccharides, proteins, and/or amino sugars. These compounds are present in the bacterial cell wall and released during the endogeneous growth phase in biological wastewater treatment processes. Major components found in the bacterial cell wall are peptidoglycans, a combination of proteins and polysaccharides. Of these, N-acetyl aminosugars are mostly found in the structure of a cell wall. According to the molecular structure of N-acetylaminosugar, functional groups found in these compounds are consistent with the response from FTIR analyses. These peaks define a hydrophilic character of this fraction; they were also found in the TPI fraction at higher intensity than in the HPO fraction. A major peak found in both HPO and TPI fractions is a peak at a wave number of 1720 cm^{-1}. This peak is associated with carboxylic groups, representing a typical characteristic of humic and fulvic acids. An increase in hydrophilic character going from HPO to TPI fraction is indicated by increases in the –OH peak at 3400 cm^{-1} and the carboxylic peak at 1720 cm^{-1}. This finding reflects less aromatic, more aliphatic, higher carboxylic, and higher charge density in the TPI fraction than in the HPO fraction.

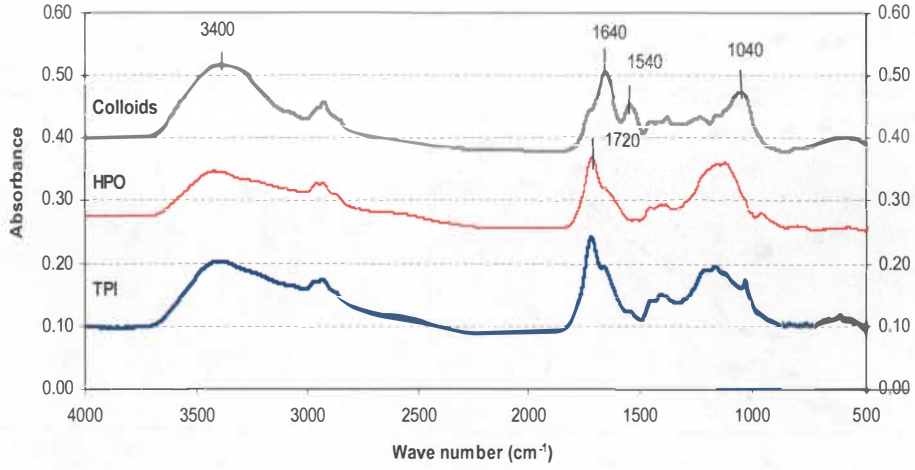

Figure 24. FTIR spectra of ST-isolates

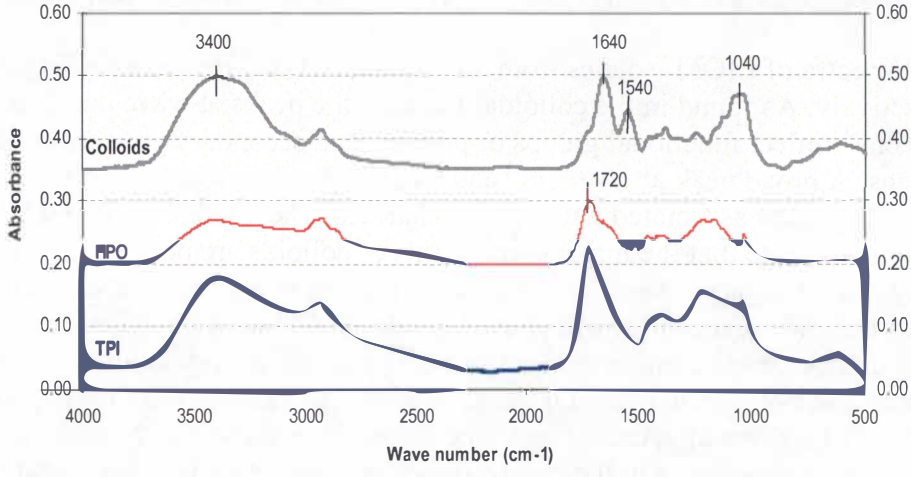

Figure 25. FTIR spectra of NA-isolates

4.2.2 Membrane properties

Membrane properties were characterized by several methods as described by Cho (1998). Each membrane exhibited various properties, resulting in differences of fouling potential and membrane rejection performance. Table 13 summarizes the properties of membranes employed in this study.

Table 13. Properties of membranes

Membrane	Type	Material	MWCO	Contact angle	Zeta potential at pH 7	PWP
			(dalton)	(°)	(mV)	(L/m^2-day-kPa)
TFC-ULP	RO					
ESNA	NF	PA	200	60.3	-11.5	1.35
GM	UF	PA	8,000	45.5	-17.0	2.96
NF200	NF	Polypiperazine	360	22.5	-15.6	0.30

Molecular Weight Cutoff. A range of polyethylene glycols (PEGs) from 200 daltons has been used for molecular weight cutoff (MWCO) determination of membranes using a dead-end stirred-cell filtration unit operated under 60 psi. A 20 mg/L concentration as DOC was used for each PEG rejection test with Milli-Q water.

Contact angle. The hydrophobicity of the membrane has been estimated by contact angle measurements using a Goniometer (Rame-Hat inc. NRL, CA).

Surface charge. The zeta potential, as calculated from the streaming potential, was measured by an electrokinetic measurement apparatus (EKA, Brookhaven Instruments Corp., Holtsville, NY) to investigate the potential for electrostatic interactions.

Pure water permeability. The pure water permeability (PWP) of a membrane is the capacity for water to pass through the membrane normalized by transmembrane pressure. This value reflects compaction of the membrane. The TFC-ULP (RO), ESNA (NF), and NF200 (NF) membranes were found to be tight membranes, whereas the GM (UF) membranes exhibited a loose structure, based on PWP.

4.2.3 Flux Decline and Membrane Fouling by EfOM Isolates

Flux decline tests were performed with a stirred cell apparatus. Flux decline by EfOM isolates was investigated by re-dissolving EfOM isolates in a mixed salt solution, consisting of $CaCl_2$, $MgSO_4$, and a phosphate buffer. The addition of inorganic salts into the synthetic source (feed) waters created similar conditions as found in wastewater effluents. Table 14 shows a composition of inorganic compounds for reconstitution of EfOM isolates. As a control experiment, the inorganic (background) solution without EfOM isolate was employed in membrane flux decline test to investigate the contribution of inorganic scale to membrane fouling. Initial DOC concentration in the feed waters was adjusted to between 4-6 mg/L. Conductivity was adjusted to approximately 500 μS/cm, reflecting an ionic strength of 0.01 M; pH was controlled by phosphate buffer at 7.0 ± 0.5. The value of total hardness of the samples was 130 mg/L as $CaCO_3$.

Various EfOM isolates would be expected to exhibit different flux decline trends based on their contributions to fouling. Generally, organic fouling of membranes is caused by adsorption, pore blockage, charge interactions, and hydrophobic interactions. Flux decline trends of TFC-ULP (RO) membranes with EfOM-isolates from ST-SE and NA-

SE are illustrated in Figures 26 (a) and (b), respectively. The results derived from the various ST-isolates generally did not show significant differences in flux decline, although the colloidal fraction tended to exhibit higher flux decline near the end of the test. However, among NA-isolates, colloids exhibited a larger flux decline than the HPO and TPI fractions. These results can be explained by the colloidal fraction being rejected by the TFC-ULP membrane and retained on the membrane surface as a cake/gel layer. Membrane resistance due to cake/gel layer formation increased, causing a reduction of permeate flux. However, the HPO and TPI fractions (i.e., EfOM acids) possessed a negative charge, and therefore less accumulation of the HPO and TPI fractions occurred on the TFC-ULP membrane due to electrostatic repulsion by the negatively charged membrane surface. It is noteworthy that the flux decline trend of the background water, i.e. inorganic dilution water, provides an indication of magnitudes of scaling versus organic fouling.

Table 14. Inorganic Matrix Composition for Reconstitution

Inorganic components	Concentration (mg/L)	Source
K^+	78	KH_2PO_4
Na^+	32	NaCl, Na_2HPO_4
Ca^{2+}	27	$CaCl_2$
Mg^{2+}	11	$MgSO_4$
Cl^-	32	NaCl, $CaCl_2$
SO_4^{2-}	50	$MgSO_4$
PO_4^{3-}	63	KH_2PO_4, Na_2HPO_4

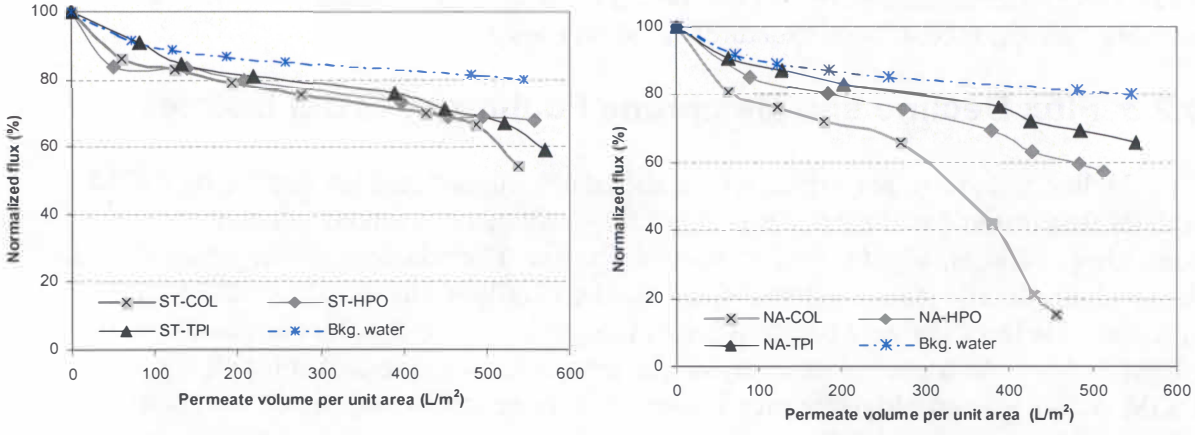

(a) ST-isolates (b) NA-isolates

Figure 26. Flux decline trends of the TFC-ULP (RO) membranes with different EfOM isolates

Figure 27a illustrates flux decline trends of the ESNA membrane with EfOM isolates from ST-SE. Large differences in flux decline trends were not observed because all fractions could be retained by the low-MWCO ESNA membrane, as described by steric

effects. Figure 27b shows flux decline trends of NA-isolates for the ESNA membrane. The colloids exhibited a larger flux decline trend than the HPO and TPI fractions. A major mechanism contributing to high flux decline by EfOM-isolates on the ESNA membrane is likely due to be pore blockage and/or cake/gel layer formation. Due to the large molecular weight of EfOM fractions compared to molecular weight cutoff (MWCO) of the membrane, an accumulation of organic molecules occurred, leading to a resistance from a cake/gel layer. Flux decline for the ESNA membrane associated with HPO and TPI fractions was smaller than that of the colloids. The HPO and TPI fractions possessed high negative charge due to deprotonated carboxylic groups, and electrostatic repulsion effects between the membrane surface and the HPO (and TPI) acids may reduce the accumulation of organic molecules. In comparison to the TFC-ULP membrane, the results with the ESNA membrane show a greater magnitude of organic fouling. The ESNA membrane possessed a high hydrophobic character based on contact angle, therefore, hydrophobic interactions likely caused more fouling with the HPO and TPI fractions for the ESNA membrane, by creating a cake/gel layer.

Figures 28a and 28b show flux decline trends for the GM membrane with the ST- and NA-isolates, respectively. Colloids exhibited a larger flux decline than the other fractions due to a deposition of this fraction; a cake/gel layer associated with hydrophilic colloids/macromolecules was formed on the membrane surface, causing high membrane resistance and flux decline. The HPO and TPI fractions exhibited a smaller flux decline due to their smaller molecular sizes compared to membrane pores. Additionally, the effects of electrostatic repulsion led to less accumulation of organic compounds on the membrane surfaces. Therefore, the differences in flux decline trends for the GM membrane between the colloids and the HPO (and TPI) fractions can be explained by both charge interactions and size exclusion effects.

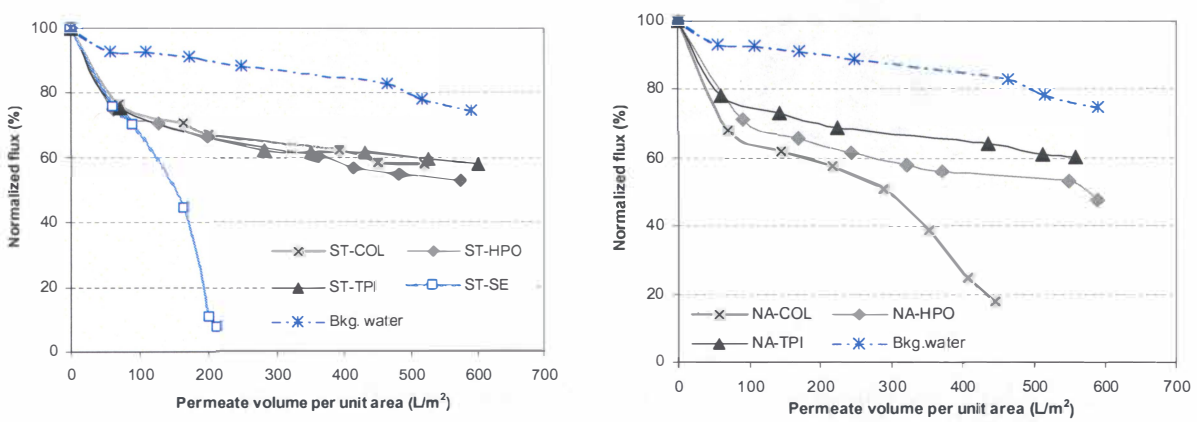

(a) ST-isolates (b) NA-isolates

Figure 27. Flux decline trends of the ESNA (NF) membranes with different EfOM isolates

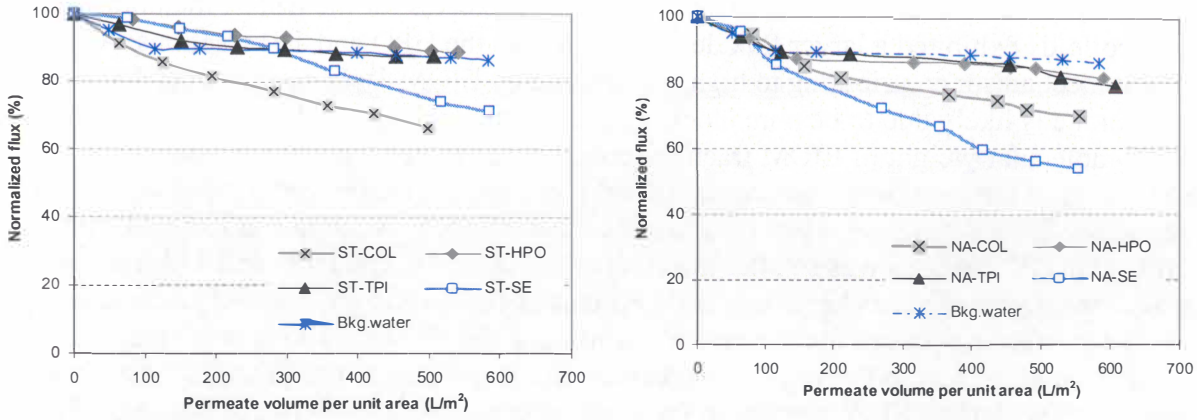

(a) ST-isolates (b) NA-isolates

Figure 28. Flux decline trends of the GM (UF) membranes with different EfOM isolates

The MFI of ST- and NA-isolates in the filtration tests with different membranes are illustrated in Figures 29a and 29b, respectively. The MFI describes the fouling potential of each EfOM-isolate for a given membrane. The results indicate a significant fouling potential of the colloidal fraction with the UF membrane. The HPO fraction exhibited a large effect with the ESNA membrane, a hydrophobic membrane, due to hydrophobic interactions.

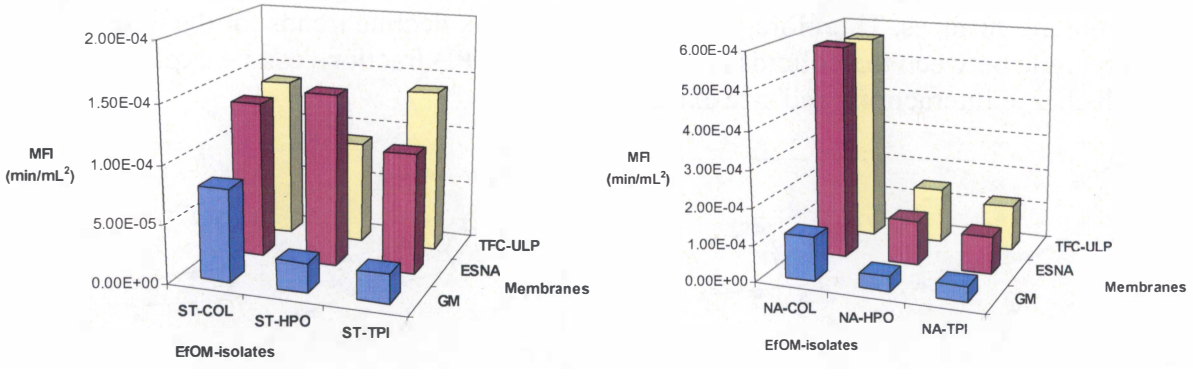

(a) ST-isolates (b) NA-isolates

Figure 29. Modified fouling index (MFI) of EfOM-isolates with different membranes

4.2.4 SEC Chromatograms of Feed, Permeate, and Retentate Streams

The results from size exclusion chromatography (SEC) analysis of each EfOM-isolate feed, permeate, and retentate support the evidence of membrane fouling and organic rejection. Figures 30a, b, and c illustrate DOC chromatograms of colloidal, HPO, and TPI fractions, respectively, in feed water compared to permeate through the TFC-ULP membrane and to organic constituents in the retentate. According to the SEC spectra, most components of EfOM isolates disappeared after passing through the membrane,

reflecting a high rejection capacity by the membrane. As described earlier, two major mechanisms in organic matter rejection are size exclusion and charge repulsion effects. The DOC chromatogram of retentate colloids indicates that the proportion of the high MW fraction decreased significantly, reflecting an accumulation of colloids on the membrane surface. Membrane resistance due to cake/gel layer formation became higher as colloids deposited on the membrane surface, causing a concomitant decrease of permeate flux. The DOC chromatograms of the HPO and TPI fractions in the retentate show that the proportions of humic-like materials do not decrease. This finding indicates low accumulation of the HPO and the TPI fractions and high organic matter rejection due to the charge repulsion mechanism.

Figures 31a, b, and c illustrate DOC chromatograms of three EfOM-isolates, including colloids, HPO, and TPI fractions, in feed water, permeate, and retentate with the ESNA membranes. The results exhibited similar trends as the TFC-ULP membranes. Most fractions were rejected by the ESNA membrane as indicated by the flat spectra of permeates. An accumulation of colloids and some HPO and TPI fractions led to pore blockage, cake layer formation, and/or gel layer formation. The chromatograms of retentates show that the HPO and TPI fractions were rejected by electrostatic repulsion and retained in the retentate portion, reflecting less accumulation of these fractions on the ESNA membrane. Conversely, the colloidal fraction was rejected by size exclusion, leaving deposited materials in membrane pores and/or on the membrane surface. The cake/gel layer of the colloidal fraction caused an increase of membrane resistance and consequently a decrease of permeate flux.

Figures 32a, b, and c show a comparison of DOC chromatograms between feed, permeate, and retentate of colloids, HPO, and TPI fractions, respectively, for the GM membrane. The colloidal fraction was totally rejected by the GM membrane, however, small molecular weight compounds still remained in the permeate portion due to the higher MWCO of the GM membrane compared to those of the TFC-ULP and ESNA membranes. The proportion of colloids in retentate became smaller compared to corresponding feed water, representing pore blockage and/or cake/gel layer formation by the colloidal fraction on the GM membrane. The proportion of humic-like materials became higher in the retentate, indicating less membrane deposition of the HPO and TPI fractions.

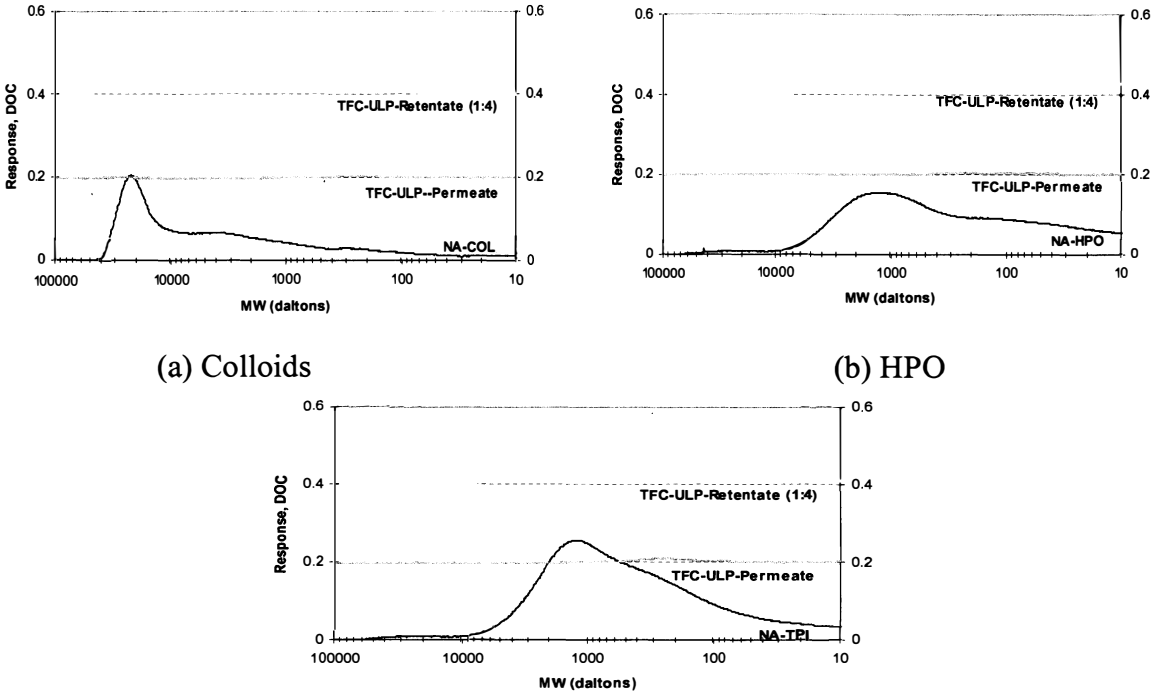

(a) Colloids (b) HPO

(c) TPI

Figure 30. SEC chromatograms of EfOM isolate feed water, and permeate, and retentate by TFC-ULP (RO) membrane (dilution factor for the retentate is 1:4)

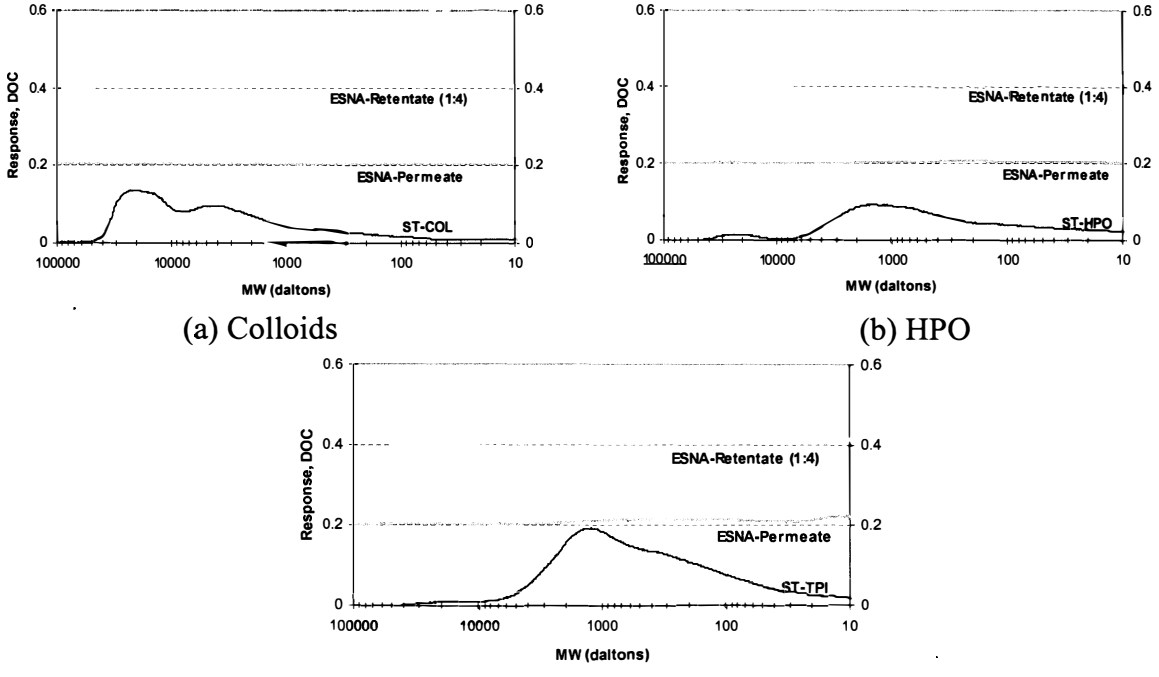

(a) Colloids (b) HPO

(c) TPI

Figure 32. SEC chromatograms of EfOM isolate feed water, and permeate, and retentate by ESNA (NF) membrane (dilution factor for the retentate is 1:4)

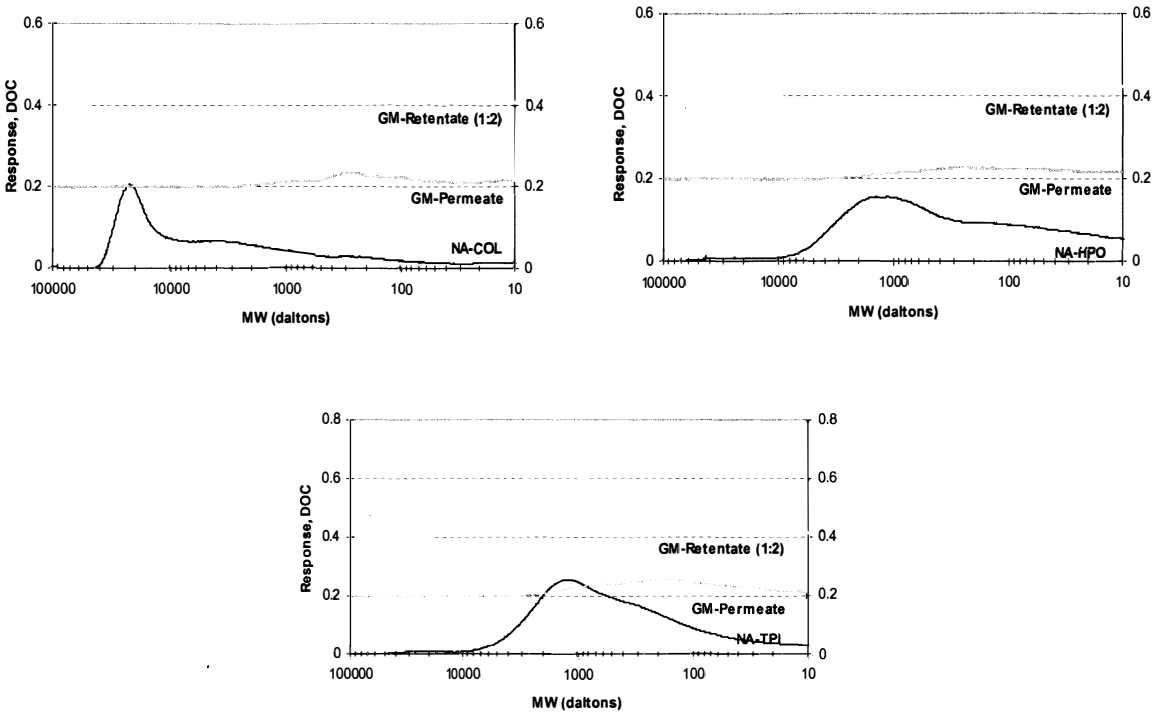

(c) TPI

Figure 33. SEC chromatograms of EfOM isolate feed water, and permeate, and retentate by GM (UF) membrane (dilution factor for the retentate is 1:4)

4.2.5 Membrane Autopsy by FTIR

An autopsy of fouled membranes was conducted using attenuated total reflection-Fourier transform spectroscopy (ATR-FTIR). The FTIR spectra identified functional groups of organic materials deposited on the membrane surface. When a membrane was fouled, the FTIR peaks of the clean membrane were changed in absorbance intensity, indicating the coverage of the original clean surface by functional groups associated with foulants. Figures 34 and 35 illustrate the IR peaks of the TFC-ULP, ESNA membranes, respectively, fouled by different EfOM-isolates compared to clean membranes. The membranes fouled with colloids exhibited significant FTIR peaks at wave numbers of 1640, 1550, and 1040 cm-1, indicating foulants with signatures corresponding proteins, polysaccharides, and/or aminosugars (Leenheer et al, 2000). These results are consistent with the FTIR spectra exhibited by the colloidal isolates and are attributable to accumulation on the membrane surface of colloids as a cake/gel layer. The peak at a wave number of 1720 cm-1 indicated minor fouling by the HPO and TPI fractions, caused by hydrophobic interactions and producing a resistance due to a gel layer on the membrane surface. The FTIR spectra of HPO and TPI fouled membranes showed peaks at wave numbers of 1640 and 1550 cm-1, reflecting proteins and/or amino sugars as major foulants, likely in the form of moieties bound to a humic structure. Figure 36 shows the FTIR spectra of the clean GM membrane compared with the GM membrane

fouled by the EfOM isolates. The results indicate that colloids are a major foulant as shown by the peaks at wave numbers of 1640, 1550, and 1040 cm-1.

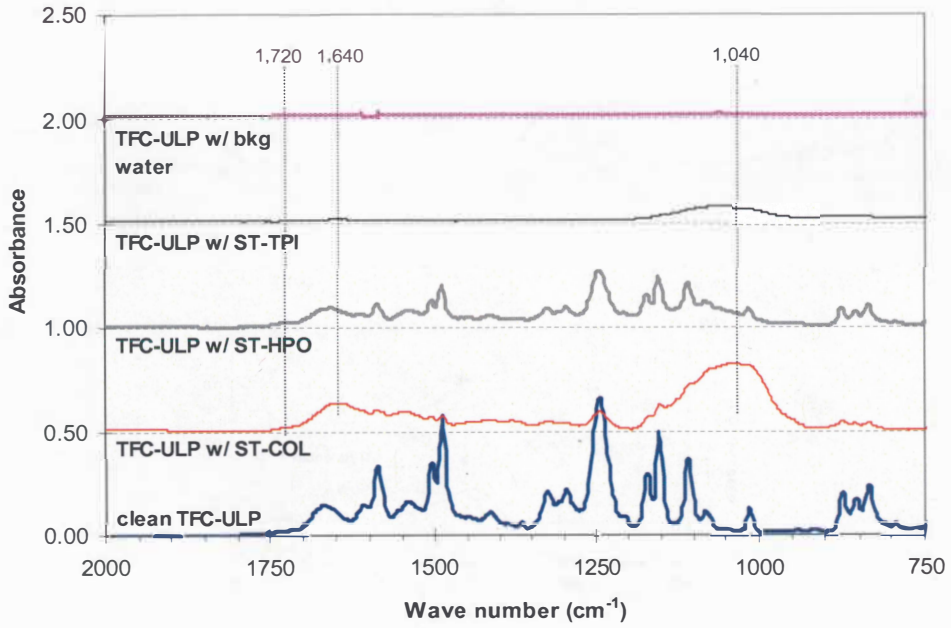

Figure 34. FTIR spectra of clean TFC-ULP membrane and the TFC-ULP membranes fouled by EfOM isolates

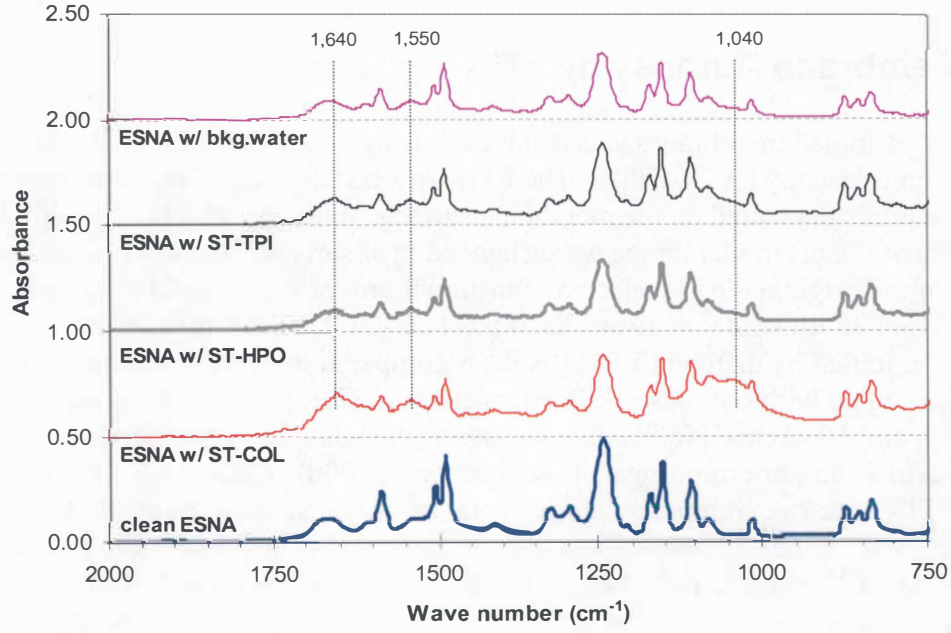

Figure 35. FTIR spectra of clean ESNA (NF) membrane and the ESNA membrane fouled by EfOM isolates

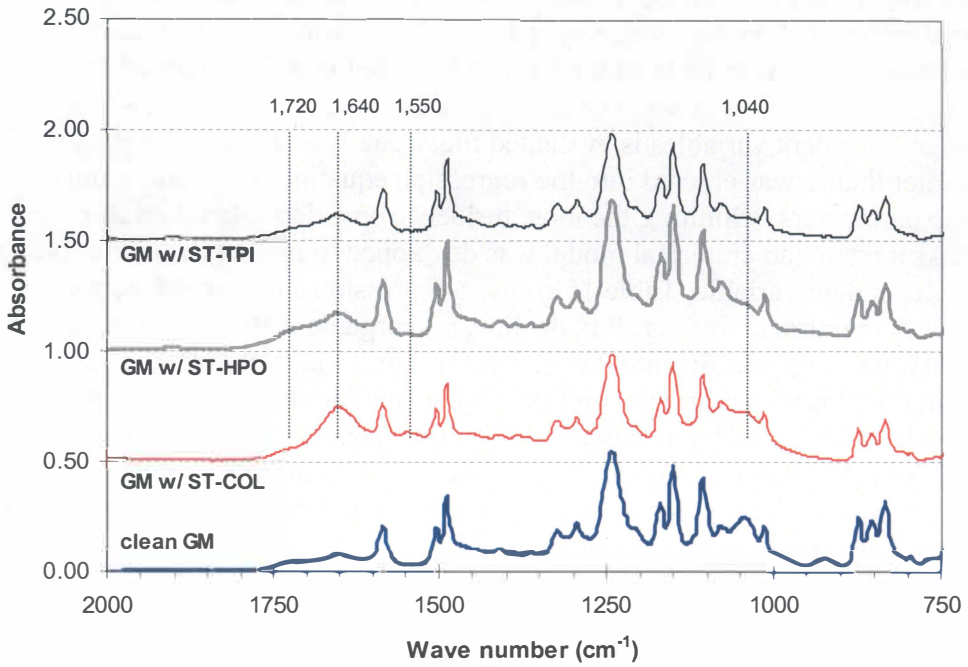

Figure 36. FTIR spectra of clean GM (UF) membrane and the GM membrane fouled by EfOM isolates

4.2.6 Multiple Regression Analysis

Multiple regression analysis was performed using STATISTICA software to analyze the relationships between several independent variables and a dependent variable. Multiple regression constructs a linear equation containing variables with a corresponding correlation coefficient indicating how well data fit the resultant model (equation). The following dependent variables were evaluated in forward step-wise multiple regression analysis:

- Modified fouling index (MFI), an index of membrane fouling, expresses the potential for fouling by a feed water on a given membrane.
- Flux decline index indicates the percent flux decline when a designated permeate volume of 1 L (350 L/m^2) is achieved.
- Permeate volume index (L/m^2) represents the volume of permeate through a given membrane when 20% flux decline is reached.
- Percent organic matter rejection is a mean value of organic rejection based on delivered DOC.

A correlation matrix of inter-variables was determined. A correlation coefficient of a dependent variable to a given independent variable exhibits how the dependent variable influences the independent variable. In the multiple regression analysis, the forward stepwise method was performed on the data set. With this method, the independent variables at each step were evaluated, and can be added or deleted from the model

depending on specified criteria, i.e. F-value. The F-value determines how significant (F to enter) or insignificant (F to remove), respectively, the contribution of a variable in the regression equation needs to be in order for it to be added or to be removed from the equation. The "F to enter" was set at one, whereas the "F to remove" was set at zero. Each of the independent variables is evaluated individually and the variable which has a F-value greater than 1 was entered into the regression equation. In the subsequent analysis, the parameters exhibiting the most influence on a dependent variable were identified. As a result, an empirical model was developed to predict a quantitative result for a given dependent variable. Table 15 shows a regression summary of equations associated with membrane fouling, flux decline, and organic matter rejection. A non-standardized regression coefficient (B coefficient) shows the relationship of a corresponding independent variable with the dependent variable. A positive value shows a positive relationship, while a negative value exhibits a negative (inverse) relationship. An adjusted R^2 value was assigned to indicate the accuracy of each predictive equation. As shown in the table, the predictive equation for MFI, as a dependent variable, shows lower accuracy compared to other indices.

Scatterplots of the predicted versus observed (measured) values are particularly useful for identifying potential clusters of cases that are not well predicted. Figures 37 through 40 illustrate scatterplots of different dependent variables associated with membrane fouling index, flux decline index, permeate volume index, and organic rejection. It is noteworthy that the area between dotted lines shows the confidence interval at 95% (α-value of 0.05).

Table 15. Regression Summary of Dependent Variables associated with Membrane Fouling, Flux Decline, and Organic Rejection

Equation	Dependent variable	Independent variable	Regression coefficient (b)	p-level	Adjust R2
1	Modified fouling index (MFI) (min/mL2)	Intercept	1.40E-03	0.006	0.66
		Zeta Potential (neg. value)	3.60E-05	0.000	
		Mass < 10 Kda	7.73E-05	0.037	
		Contact angle	-2.30E-05	0.025	
		SUVA	9.69E-05	0.017	
		SCD	-2.12E-04	0.035	
		Mass TPI	-2.24E-04	0.174	
2	Flux decline index (FDI, %)	Intercept	232.495	0.000	0.86
		Zeta Potential (neg. value)	17.159	0.000	
		Mass TPI	3.374	0.381	
		MWCO	0.009	0.000	
		PWP	-2.614	0.002	
		Mass > 10 kDa	3.606	0.041	
		UVA	64.304	0.206	
3	Permeate volume index (PVI) (L/m2)	Intercept	-1978.803	0.001	0.79
		Zeta Potential (neg. value)	-217.997	0.000	
		Mass TPI	-302.855	0.051	
		MWCO	-0.122	0.000	
		PWP	38.008	0.001	
		Mass >10 kDa	-193.330	0.010	
		TDS	-0.228	0.086	
		Mass HPO	94.492	0.257	
		SUVA	-113.302	0.090	
		UVA	1472.982	0.185	
4	Organic matter rejection (%)	Intercept	271.450	0.001	0.74
		Zeta Potential (neg. value)	17.798	0.002	
		SUVA	-10.814	0.014	
		PWP	-4.278	0.002	
		MWCO	0.010	0.010	
		Mass > 10 kDa	4.247	0.345	
		Total hardness	0.130	0.022	
		SCD	-27.183	0.038	
		Mass HPO	-2.629	0.176	

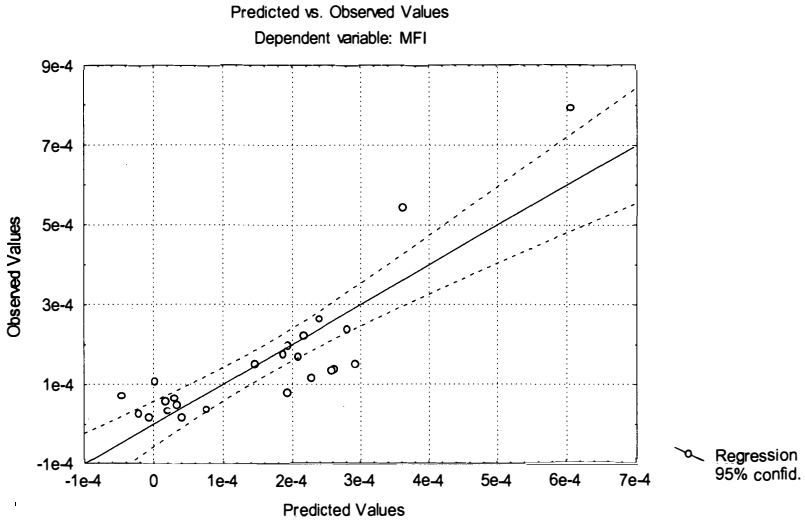

Figure 37. Scatterplot of predicted versus observed values for modified fouling index (MFI) (R2 = 0.66)

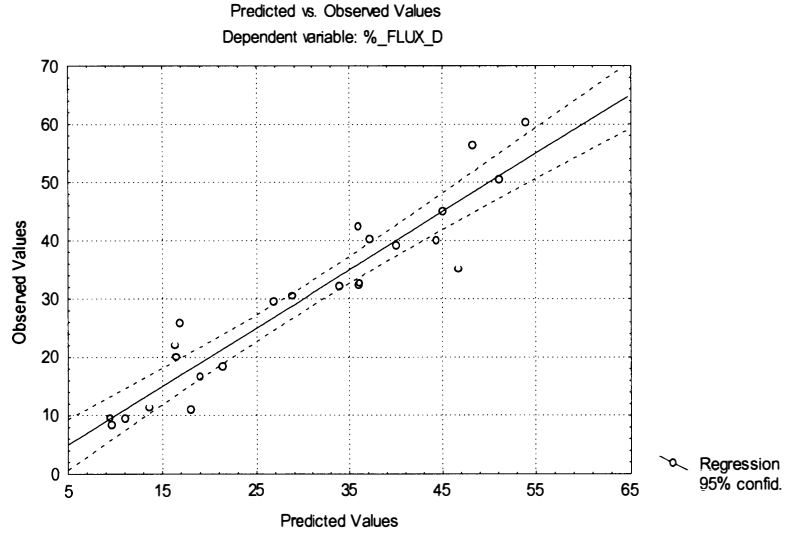

Figure 38. Scatterplot of predicted versus observed values for flux decline index (R2 = 0.86)

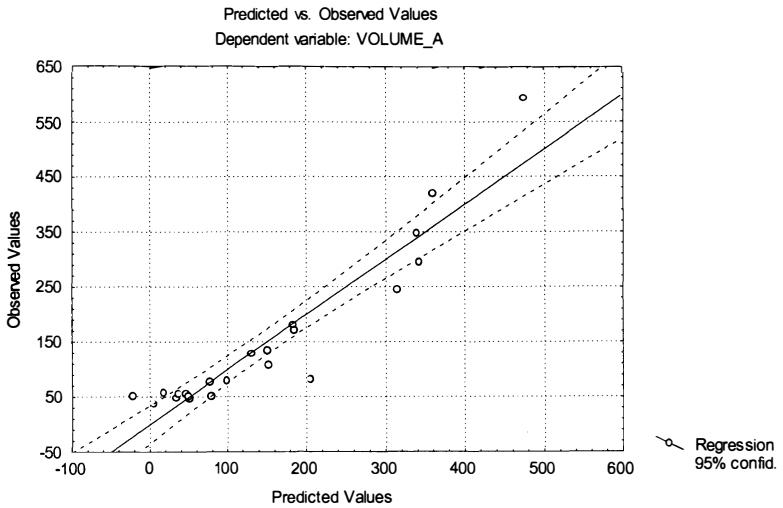

Figure 39. Scatterplot of predicted versus observed values for permeate volume index (R2 = 0.76)

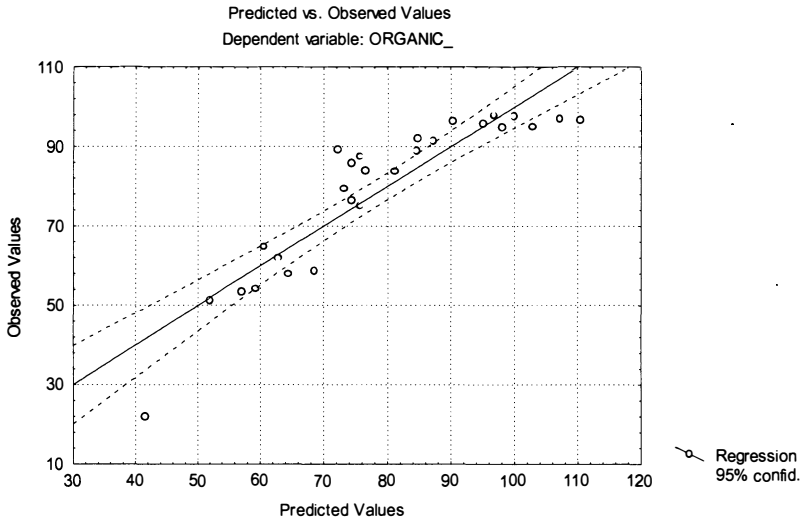

Figure 40. Scatterplot of predicted versus observed values for organic rejection (R2 = 0.74)

4.2.7 Summary

According to membrane filtration tests, EfOM isolates exhibited different behaviors in membrane fouling and flux decline. Colloids fouled the TFC-ULP (RO), ESNA (NF), and GM (UF) membranes by a major mechanism of pore blockage and/or a formation of cake/gel layer. There were no significant differences of flux decline by various isolates with the RO and NF membranes because all isolates were rejected and retained on the membrane surface. Colloids exhibited larger flux decline than the other EfOM isolates on the UF membrane because of the effects of size exclusion. The FTIR spectra of membranes fouled by colloids indicated possible foulants such as proteins, polysaccharides, and/or aminosugars. Membranes fouled by the HPO and TPI fractions

also showed peaks of proteins and/or polysaccharides as foulants but to a lesser degree than the colloidal fraction. The carboxylic peak of HPO- and TPI-fouled membranes was not apparent when compared to FTIR of the HPO and TPI isolates. Electrostatic repulsion is likely to be a major mechanism in rejection of HPO and TPI fractions, resulting in a lower flux decline. SEC chromatograms of feed, permeate, and retentate provide supporting evidence of colloidal deposition on the membrane surface and of electrostatic repulsion between the negatively charged membrane surface and the negatively charged HPO and TPI isolates (acids).

Multiple regression analysis was performed to identify the relationship of multiple independent variables associated with membrane properties and feed water characteristics. The empirical models from the analysis can be used to predict the performance of membranes regarding fouling potential, flux decline, permeate volume, and organic matter rejection. The dependent variables that were found to affect membrane performance were zeta potential, MWCO, SUVA, mass of HPO, mass of organic compounds larger than 10,000 daltons, and total hardness.

4.3 Algal Organic Matter

The work reported in this section of the report represents an extrapolation of previous work based on other classifications of organic matter, including terrestrially derived (allochthonous) natural organic matter (NOM) and wastewater derived effluent organic matter (EfOM). Another important type of organic matter is represented by algogenic or algal derived (autochthonous) organic matter (NOM). The hypothesis is that AOM reflects important similarities and differences with NOM and EfOM. Along with EfOM, it represents microbially derived organic matter. In contrast to NOM, it represented less aged and humidified organic matter. In the previous progress report, we presented results of membrane filtration experiments performed with AOM, but with incomplete characterization information. In order to provide a comprehensive overview, we are re-presenting the membrane filtration results along with recently completed characterization work.

The aims of this part of the study were to characterize AOM by various methods and to evaluate NF membrane fouling associated with AOM. For these experiments, the membrane employed was NF 200, having polypiperazine as an ultrathin top layer, a MWCO of 360 daltons determined by polyethylene glycol (PEG) rejection tests, a relatively low contact angle (22.5°), and a high negative surface charge (-16.5 mV at pH 7.0 and 300 μS/cm with KCl). The NF 200 membrane would be expected to cause less hydrophobic interactions that might lead to flux decline with hydrophobic NOM, and to reject well negatively charged NOM components (e.g., humic and fulvic acids) by electrostatic repulsion. Therefore, AOM that contains large amounts of proteins and polysaccharides may cause significant fouling of the NF 200 membrane due to its charge, hydrophilicity, and size of the AOM.

4.3.1 Materials and Methods

AOM Extraction and Preparation for Analyses Blue green (B-G) algae were obtained from Klamath Blue Green Inc., CA. They were harvested from Klamath Lake located in the Cascade Mountains of Southern Oregon; their morphological, biochemical, and immunological properties appeared to be mostly retained by the freeze-drying method. The composition of the B-G algae consists of 68 % protein, 22 % carbohydrate, 5 % lipids, and 3 % chlorophyll a (reported by the supplier). Extraction of AOM was performed using 0.45 μm cartridge (nylon filter) filtration. G-AOM corresponds to AOM extracted in water after physically grinding algal cells with a mortar and pestle while S-AOM corresponds to AOM extracted in water after ultrasonification of algal cells in water for 1 hour. AOM-Me is AOM extracted in 90 % methanol over 24 hours. Chlorophyll a extracted from Anacystis nidulans algae was obtained from Sigma to help identify the AOM components by the UV/visible analyses. Chlorophyll a was dissolved in 90 % methanol solvent.

The AOM dissolved in water after grinding the B-G algae was fractionated according to size using 0.45 μm (Nylon) and 1.2 μm (GF/C, Glass Fiber) filters and solidified for functional group identification by FTIR.

Synthetic Water Samples. Synthetic water samples were prepared with different blends of Suwannee River humic acid (SRHA) and S-AOM solutions to evaluate the effects of two different sources/types of organic matter on NF (NF 200) membrane fouling under the same conditions. The pH and conductivity were adjusted with H_2SO_4, NaOH, and Na_2SO_4 (pH 6.8 and 300 μS/cm) and the DOC concentration of synthetic waters was set to 10 mg C/L (SRHA 10 mg C/L, AOM 3 mg C/L + SRHA 7 mg C/L, AOM 7 mg C/L + SRHA 3 mg C/L, and AOM 10 mg C/L).

Sample Analyses. Organic matter analysis included dissolved organic carbon (DOC) and ultraviolet absorbance (UVA) at the wavelength of 254 nm, with specific UV absorbance representing the ratio of UVA254 to DOC. NOM fractionation in feed waters was performed by XAD-8/-4 resin adsorption that defined the distribution of mass fraction in terms of hydrophobic (HPO) vs. transphilic (TPI) vs. hydrophilic (HPI) DOC. UV absorbance spectra for AOM samples have been also obtained by scanning from 200 to 700 nm with a UV-visible spectrophotometer.

ATR-FTIR was performed to identify the functional groups of various solid samples and fouled membranes; the method was described in previous progress reports. HPSEC-UV-fluorescence-DOC was employed to estimate molecular weight distributions as a function of three difference detectors. Analysis was performed according to methods described in previous progress reports; the excitation and emission wavelengths for fluorescence were chosen to detect protein-like substances. The fluorescence excitation-emission matrix (EEM) spectra were measured over a range of excitation and emission wavelengths, with the intensity of EEM is represented by contour lines. The method was described in previous progress reports.

Membrane Test Unit. A Millipore Mini-Tan system (a bench-scale cross-flow unit employing a flat-sheet membrane specimen) was used to perform bench-scale flux decline and rejection experiments with the NF 200 membrane. The Mini-Tan system and the associated bench-scale protocol have been described in previous progress reports.

4.3.2 Results and Discussion

Characteristics of AOM Feed waters were synthesized to reflect varying proportions of SRHA and S-AOM, selected because ultrasonification was considered to more representative of cell lysis. Water quality parameters of feed waters are summarized in Table 16. The specific UVA (SUVA, representing an index of NOM aromaticity) values of SRHA and S-AOM were 7.4 L/m-mg and 1.0 L/m-mg. AOM exhibits a much lower aromaticity compared to SRHA. Table 2.2 shows the distribution of DOC fractions for SRHA and AOM. The HPI fraction was high for AOM (57.3 %) while SRHA, as expected, showed a high HPO fraction (93.5 %) (Table 17). The HPO fraction can potentially exhibit high hydrophobicity associated with a high aromatic structure (high SUVA).

Table 16. Water quality of feed waters

Feed waters*	pH	Conductivity (μS/cm)	UVA_{254} (cm^{-1})	DOC (mg/L)	SUVA (L/mg-m)
SRHA 10 mg C/L	6.80	300	0.74	10	7.4
(S-AOM 3 mg + SRHA 7 mg) C/L	6.80	300	0.58	10	5.8
(S-AOM 7 mg + SRHA 3 mg) C/L	6.80	300	0.42	10	4.2
S-AOM 10 mg C/L	6.80	300	0.10	10	1.0

*DOC = 10 mg/L adjusted with H_2SO_4, NaOH, and Na_2SO_4; no Ca^{2+}

Table 17. DOC fractionation of feed waters by XAD-8/4 resins

	HPO (%)	TPI (%)	HPI (%)
SRHA	93.5 (0.96)	5.2 (0.49)	1.4 (0.49)
S-AOM	25.9 (1.41)	16.8 (2.69)	57.3 (4.1)

( ): Standard deviation

UV/visible absorption spectra are shown in Figure 41 for G-AOM, S-AOM, AOM-Me, and chlorophyll *a*. UV/visible spectra shows that the extraction of organic matter does not highly depend on the physical method (i.e., grinding or sonicating) but on solvents (i.e., water or methanol). The spectra were similar for G-AOM and S-AOM, extracted in water as a solvent. However, AOM-Me showed additional absorption peaks around 400 nm and at 664 nm. The absorption around 400 nm may be from chlorophyll *a*. Chlorophyll *a*, exhibiting a green color, also shows strong absorption of red light at 664 nm. Chlorophyll a appears not to be dissolved well in water as a solvent.

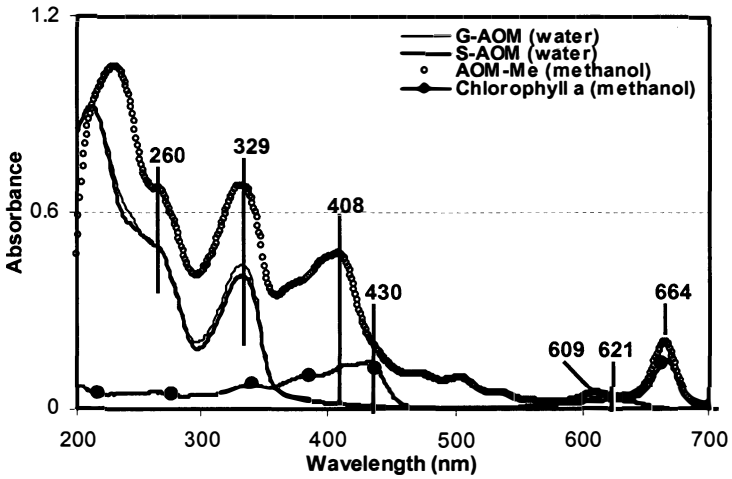

Figure 41. UV absorbance for G-AOM, S-AOM, AOM-Me, and chlorophyll *a*

Figure 42 shows HPSEC-UV-fluorescence-DOC chromatograms for S-AOM and SRHA. The results of MW estimations in Table 18 for SRHA and S-AOM were obtained using the UV and DOC spectra portrayed in Figure 41. S-AOM has a high weight-averaged MW (Mw) and low number-averaged MW (M_n) for both detectors, resulting in a high value of polydispersivity ($\rho = M_w/M_n$). S-AOM shows multiple peaks (greater heterogeneity) with a lower SUVA (maximum: 0.73 L/m-mg), compared to SRHA. On the contrary, SRHA shows a single peak around 3,400 daltons with a highest SUVA value (8.58 L/m-mg) and a low specific fluorescence intensity (0.01 height unit). The specific fluorescence is much higher for S-AOM than for SRHA, indicating a higher protein content in AOM.

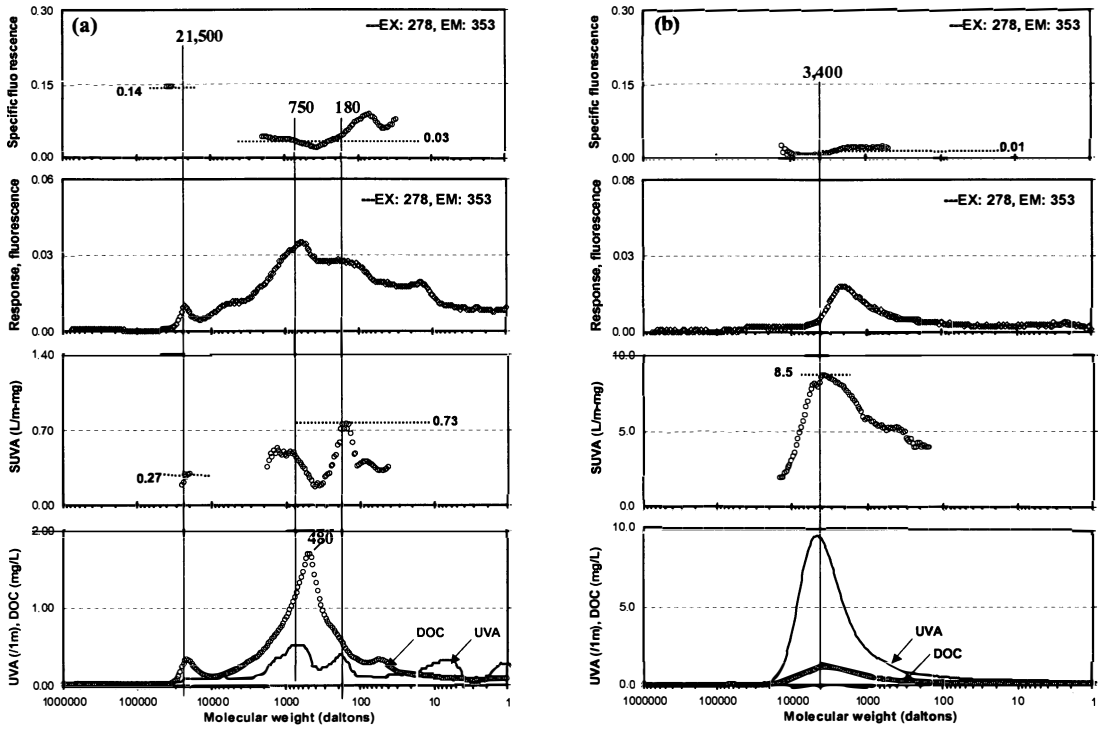

Figure 42. Chromatograms of HPLC-UV-fluorescence-DOC for (a) S-AOM and (b) SRHA.

Table 18. MWs measured by UV and DOC detectors

	Weight-averaged MW (M_w)		Number-averaged MW (M_n)		Polydispersivity (M_w/M_n)	
	UV	DOC	UV	DOC	UV	DOC
SRHA	3305	3409	1934	1730	1.7	2.0
S-AOM	1960	2250	231	263	8.5	8.6

Figure 43a shows the FTIR spectra of B-G algae, AOM materials, and SRHA. All samples displayed strong absorption bands at 3430 cm^{-1}, characteristic of hydrogen bonded OH. Relatively high aliphatic CH_2 absorption bands were seen at 2926 cm^{-1} (asymmetric stretching) and 2853 cm^{-1} (symmetric stretching) for AOM-Me. The 1720 cm^{-1} absorption bands, mainly associated with C=O of C(=O)OH, were stronger for SRHA than for all AOM materials. The absorption intensity of C(=O)OH increased in the order: B-G algae, G-AOM, S-AOM, and AOM-Me. The absorption bands at 1613-1622 cm^{-1} may be associated with aromatic C=C and ionized carboxylic acids. B-G algae showed distinctive protein peaks at 1661 cm^{-1} and 1552 cm^{-1}. Proteins, like polypeptides in general, consist of chains of amino acid residues joined end-to-end by secondary amide bonds. The absorption at 1661 cm^{-1} is the stretching vibration bands associated primarily with the peptide carbonyls (C=O, amide I band). The amide II bands are seen at 1552 cm^{-}

[1] resulted from the interaction between the N-H bending and the C-N stretching of the C-N-H group.

Figure 43 b shows the FTIR spectra of B-G algae on the basis of size after fractionation in water as a solvent following the grinding of the B-G algae. The absorption bands by hydrogen bonded NH were much stronger at 3308 cm^{-1} for the algal components above 0.45 μm and the original B-G algae, while dissolved components less than 0.45 μm (G-AOM) showed a stronger absorption by hydrogen bonded OH at 3430 cm^{-1}. The absorption by amide I and II bands also occurs significantly at 1661 cm^{-1} and 1552 cm^{-1} for the algal components above 0.45 μm. This suggests that dissolved AOM contains lower nitrogen-containing components compared to colloidal/particulate algal components. However, the content of polysaccharide-like substances observed at 1040-1150 cm^{-1} are relatively higher for dissolved AOM than larger size algal components.

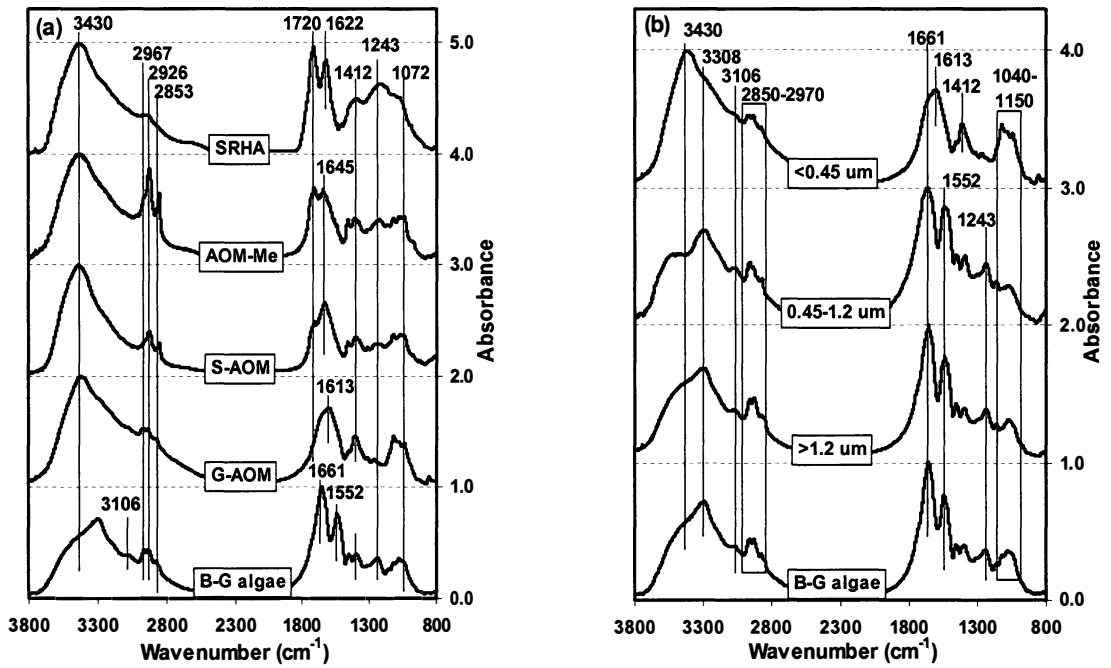

Figure 43. FTIR spectra; (a) B-G algae, G-AOM, S-AOM, AOM-M, and SRHA; (b) B-G algae depending on size (in water after grinding algae).

Figure 44 shows the EEM spectra of S-AOM (5-10 mg C/L) and SRHA (around 2 mg C/L). The EEMs show protein-like substances (at EX: 279-282 nm and EM: 304-353 nm) and humic substances (at EX: 352 nm and EM: 441 nm). The EEM peak maxima of SRHA (EX: 341 nm and EM: 453 nm) shows a red shift (longer excitation and emission wavelengths) compared to humic substances in AOM (EX: 352-360 nm and EM: 441 nm), indicating a more oxidized form of SRHA and more electron-donating substituents in AOM.

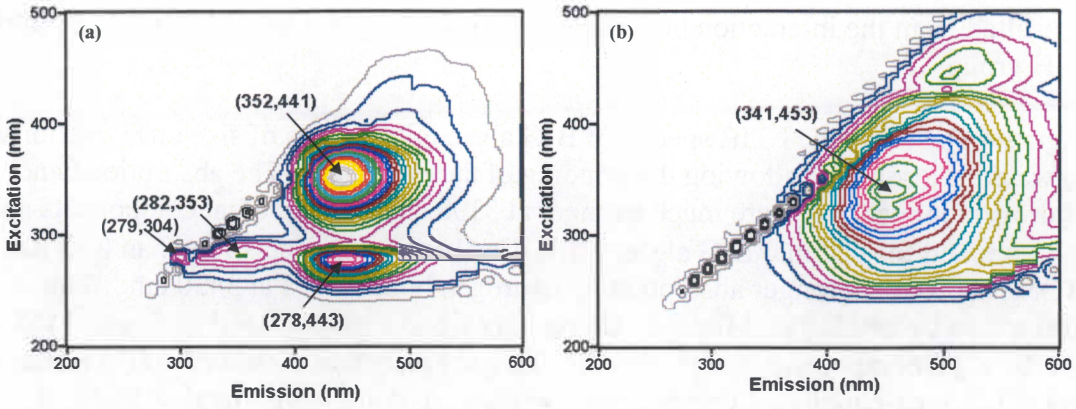

Figure 44. Fluorescence EEM of (a) S-AOM and (b) SRHA

4.3.3 Results of Membrane Tests

Flux decline and organic matter rejection were studied for each of the four blend samples of SRHA and S-AOM. Figure 45 shows the results of flux decline and organic matter rejection as a function of delivered DOC (based on summation of DOC flux in feed water) at 20 °C. Even though the test conditions were the same (NOM concentration, pH, temperature, inorganic salt concentration, and recovery), significantly different results were obtained depending on the organic matter composition of the feed waters. When 12 mg of DOC was delivered per cm^2 of membrane, flux decline was 4.4 % for the membrane fed with 10 mg C/L of SRHA only and increased up to 20.0 % for the membrane fed with 10 mg C/L of AOM only (Figure 45 a). A higher flux decline was observed with increasing AOM proportion. However, organic matter rejection measured by DOC (Figure 45 b) decreased with an increasing AOM contribution to the samples, indicating that the lower MW AOM components were not well rejected by the NF 200 having a 360 dalton MWCO.

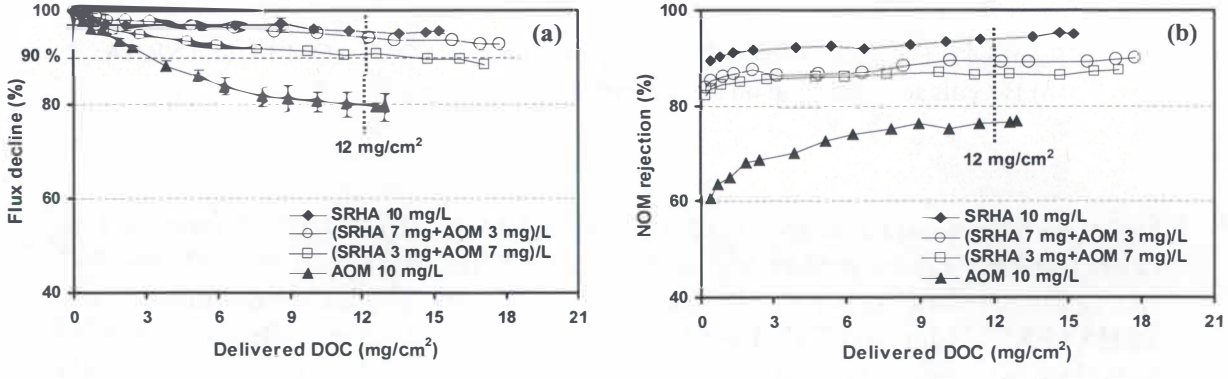

Figure 45. Flux decline and organic matter rejection (based on DOC) as a function of delivered DOC for SRHA, AOM, and blend samples.

The DOC and SUVA values of membrane permeate are shown in Figure 46 as a function of delivered DOC. The decrease in DOC of permeate over time may be due to the additional separation by an increase in fouling. The DOC concentrations of permeate at 12 mg/cm^2 delivered DOC increased from 0.45 mg/L with SRHA only to 1.34 mg/L with AOM only. Permeate SUVA values were highly dependent on those of the corresponding feed water: 3.01 L/mg-m with SRHA only and 1.04 L/mg-m with AOM only, respectively.

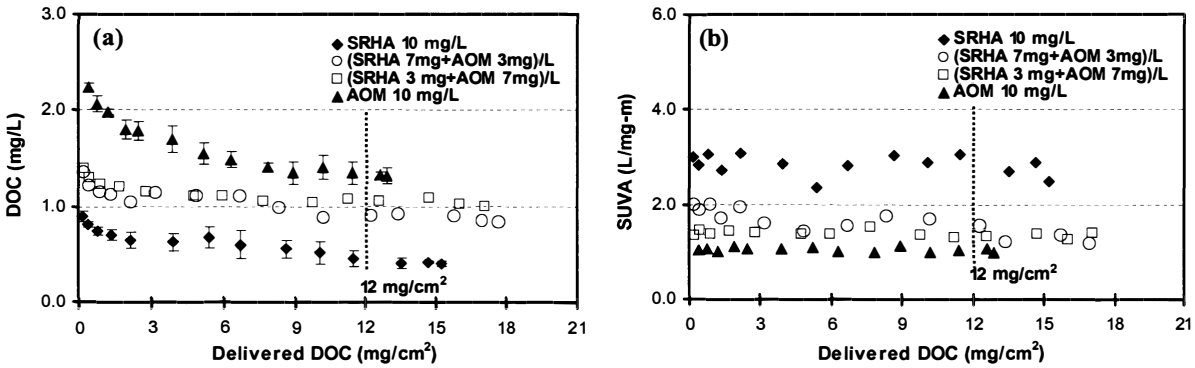

Figure 46. Permeate quality as a function of delivered DOC: (a) DOC and (b) SUVA

The FTIR spectra of clean and fouled membranes were compared in Figure 47. A C=O stretching peak from carboxylic acid was seen at 1740 cm^{-1} from the membrane fouled with SRHA 10 mg C/L. However, with the increase of AOM proportion, this peak was not clearly seen probably due to a higher intensity peak at 1650 cm^{-1} corresponding to a stretching vibration of C=O connected to amides from AOM. The C=O stretching vibration is coupled with the adjacent N-H bending vibration peak appearing at 1550 cm^{-1} (N-H stretching: 3300 cm^{-1}). The peak near 1000-1120 cm^{-1} is associated with alcoholic C-O absorption. Alcoholic C-O bonds may originate from polysaccharide-like substances. Both protein and polysaccharide like substances were found as major foulants whose FTIR peaks were more significant for fouled membranes associated with AOM.

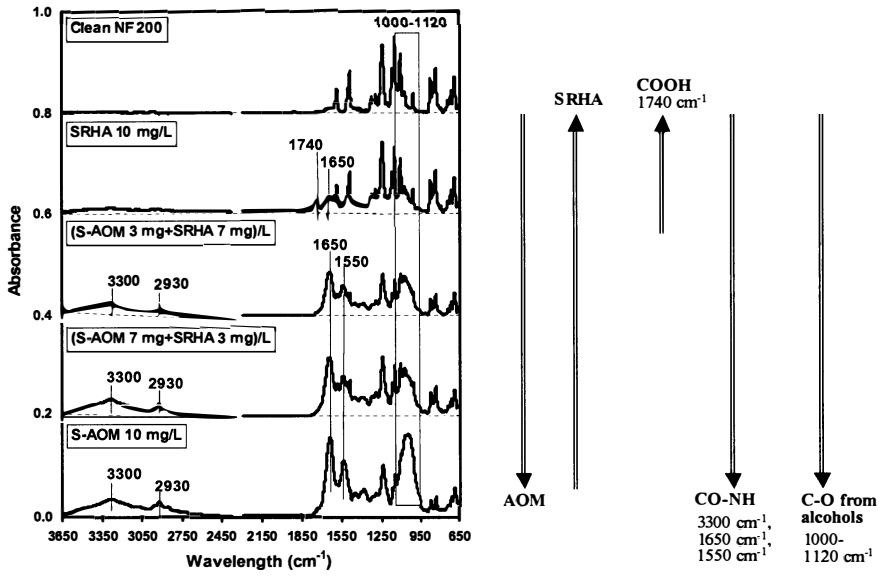

Figure 47. FTIR spectra of membranes (NF 200) fouled by SRHA, S-AOM, and blend samples

4.3.3 Summary

AOM showed a high HPI fraction (57.3 %) and a low SUVA (1.0 L/m-mg). MW distribution showed a greater heterogeneity (high value of polydispersivity) and higher protein content for 21,500 dalton components (by specific fluorescence). The existence of protein was proven by FTIR (at 1661 cm^{-1} and 1552 cm^{-1}) and EEM (EX: 278-282 nm and EM: 304-353 nm). However, SRHA showed a high HPO fraction (93.5 %) with high SUVA (7.4 L/m-mg). A large amount of C(=O)OH functional groups (at 1720 cm^{-1}) and aromatic rings (at 1622 cm^{-1}) was found by FTIR in SRHA.

Our observations in membrane tests suggest that (negatively charged) humic substances of relatively high MW (5,000-1,000 daltons) and high SUVA were preferentially rejected through electrostatic repulsion/size exclusion by the NF 200 membrane, having a high negative charge (zeta potential: -15.6 mV), low MWCO (360 daltons), and relatively low hydrophobicity. However, in the case of AOM that reflects a wide MW range of components with less aromatic and more hydrophilic fractions, the NF 200 membrane showed high fouling and poor rejection (the smaller constituents passed through the membrane). Even though the DOC concentration of feed water is a decisive factor for membrane fouling in addition to membrane properties and operating conditions, the characteristics of organic matter is more likely associated with fouling potential. Protein-like and polysaccharide-like substances were found as major foulants by FTIR.

5. References

Aiken, G, R., and Leenheer, 1993, Chemistry and Ecology, 8, 135-151.

Aiken, G. R., Humic Substances and their role in the environment, 1988, John Wiley & Sons Limited, 15-28.

Aiken, G. R., McKnight, D. M., Thorn, K. A., Thurman, E. M., 1992, Organic Geochemistry, 18(4), 567-573.

Aiken, G. R., Thurman, E. M., and Malcolm, R. L., 1979, Analytical Chemistry, 51(11), 1799-1803.

Babel, S., Takizawa, S., Ozaki, H., 2002, Wat. Res., 36, 1193-1202.

Carroll, T., King, S., Gray, S.R., Bolto, B.A., and Booker, N.A. (2000), Wat. Res., 34(11), 2861-2868.

Combe, C., Molis, E., Lucas, P., Riley, R., and Clark, M. (1999), J. of Mem. Sci., 154, 73-87

Fan, L., Harris, J., Roddick, F., and Booker, N. (2001), Wat. Res., 35(18), 4455-4463.

Her, N, Ph.D dissertation, 2002, U of Colorado at Boulder.

Her, N., Amy, G., and Jarusutthirak, C., Desalination, 2000, 132, 143-160.

Her, N., Amy, G., Foss, D., Cho, J., Yoon, Y., and Kosenka, P., Envrion. Sci. Tech. 2002, Vol 36, pp. 1069-1076.

Howe, K. J., and Clark, M. M., Environ. Sci. Technol., 2002, 36, 3571-3576.

Huber, S.A., Desalination, 1998, 119, 229-234.

Jarusutthirak, C, Ph.D dissertation, 2002, U of Colorado at Boulder.

Jarusutthirak, C., Amy, G., and Croue, Jean-Philippe, Desalination, 2002, 145(1-3), 247-255.

Jones, K. and O'Melia, C. (2000), J. of Mem. Sci., 165, 31-46.

Laabs, C., Personal communication, 2003.

Lee, N., Makdissy, G., Amy, G., Croué, J-P, Buisson, H., and Schrotter, J-C (2003), Proceeding-AWWA Mem. Tech. Conf. (MTC), T3.

Lin C.F., Lin T. Y., and Hao, O.J. (2000), Wat. Res., 34(4), 1097-1106.

Platt, T, Fuentes-Yaco, C, Frank, K. T., Nature, 2003, 423, 398-399.

Reichenbach, C., Jekel, M., and Amy, G., 2001, Proceedings – AWWA, Water Quality Technology Conference, 303-314.

Silverstein, R. M., Webster, F. X., Spectrometric identification of organic compounds, 6th edition, Chapter 3. 1998, John Wiley & Sons, Inc.

Thurman, E. M., Malcolm, R., and Aiken, G. R., 1978, Analytical Chemistry, 50(6) 775-779.

Torokne, A., Palovics, A., Bankine, M., Environ. Toxicology, 2001, 16, 512-516.

Yuan, W., Zydney, A. (1999), J. of Mem. Sci., 157, 1-12.

Zeman, L. and Zydney, A., Marcel Dekker, Inc., 1996.